Modeling different freeze/thaw processes in heterogeneous landscapes of the Arctic polygonal tundra using an ecosystem model

Shuhua Yi[1,2], Karoline Wischnewski[2], Moritz Langer[2], Sina Muster[2], and Julia Boike[2]

[1]{State Key Laboratory of Cryospheric Sciences, Cold and Arid Regions Environmental and Engineering Research Institute, 320 Donggang West Road, 730000, Lanzhou, Gansu, China}

[2]{Alfred Wegener Institute for Polar and Marine Research, Telegrafenberg A43, 14473 Potsdam, Germany}

Correspondence to: S. Yi (yis@lzb.ac.cn)

Abstract

Freeze/thaw (F/T) processes can be quite different under the various land surface types found in the heterogeneous polygonal tundra of the Arctic. Proper simulation of these different processes is essential for accurate prediction of the release of greenhouse gases under a warming climate scenario. In this study we have incorporated the water layer into a dynamic organic soil version of the Terrestrial Ecosystem Model (DOS-TEM), having first verified and validated the model. Results showed that (1) the DOS-TEM was very efficient and its results compared well with analytical solutions for idealized cases, and (2) despite a number of limitations and uncertainties in the modeling, the simulations compared reasonably well with *in situ* measurements from polygon rim, polygon centers (with and without water), and lake on Samoylov Island, Siberia. We concluded that the DOS-TEM is suitable for simulating the various F/T processes. Sensitivity tests were then performed on the effects of water depth. Our results indicated that water, as well as snow cover, are very important in the simulated thermal processes for both polygon centers and lakes. We therefore concluded that the polygon rims and polygon centers (with various maximum water depths) should be considered separately, and that the dynamics of water depth in both polygons and lakes should also be taken into account when simulating thermal processes for methane emission studies.

1 Introduction

The release of greenhouse gases from the large quantities of soil carbon preserved in Arctic regions constitutes an important feedback to climatic warming and the thawing of permafrost north of 45^{o}N (McGuire et al., 2009; von Deimling et al., 2012). Reliable simulation of the dynamics of permafrost is therefore critical when predicting future climatic changes. The energy balance at the ground surface has an important influence on variations in permafrost. Heterogeneous ground surfaces with (e.g., variable snow pack thicknesses and organic layer thicknesses) exert a major influence on the surface energy balance (Etzelmüller and Frauenfeld, 2009) and have in the past been integrated into both land surface models (Yi et al, 2007; Lawrence and Slater, 2008) and ecosystem models (Zhuang et al., 2001; Yi et al., 2009a,b; Yi et al., 2010). However, few of the current large scale land surface models or ecosystem models take into account the effects that water bodies have on the dynamics of permafrost (Zhuang et al., 2006; Ringeval et al., 2012), with one exception being the model by Wania et al. (2009) which treated surface water in the same way as a litter layer. Water bodies of various sizes, ranging from those occupying polygon centers to large thermokarst

lakes, are distributed across the Arctic coastal regions (French, 2007) resulting in considerable landscape heterogeneity. Water bodies have a marked effect on the surface energy balance and thermal dynamics of the surrounding permafrost soils (French, 2007). Their presence can lead to permafrost degradation, which in turn affects the terrestrial ecosystem's carbon budget. Outgassing of carbon dioxide from ponds and lakes was, for example, calculated to account for between 74 and 81% of the net landscape-scale CO_2 emissions in polygonal tundra in the Lena Delta (Siberia) (Abnizova et al., 2012).

There are a number of different techniques used to simulate permafrost dynamics (Riseborough et al., 2008). A wide range of numerical models exist, which are applied both in stand-alone permafrost simulations and in land-surface schemes of climate models. The temperature and water content at different depths in soil or rock are calculated numerically. Numerical solutions for permafrost dynamics in large scale models are commonly obtained by solving finite difference equations. One category of numerical solution, referred to by Zhang et al. (2008) as "decoupled energy conservation parameterization", assumes that the soil water is homogeneous and freezes or thaws at exactly 0^oC. Soil temperature is calculated for each layer and if the temperature of a particular layer is then greater than 0^oC, some or all of any present ice will melt and the temperature is then recalculated, and *vice versa*. This is an efficient method and is commonly used in land surface models (Zhang et al., 2003; Oleson et al., 2004). However, the lower layers in land surface models are usually thick and the freezing or thawing fronts derived from soil temperature interpolation are not realistic (Yi et al., 2006).

A second category of numerical methods, referred to by Zhang et al. (2008) as "apparent heat capacity parameterization", assumes that soil water freezes or thaws over a range of temperatures below 0^oC and simulates the unfrozen soil water content and temperature simultaneously. Since small changes in soil temperature within the freeze/thaw range will result in a large change in apparent heat capacity, an iterative procedure is required to ensure that only small temperatures changes during each time interval (Nicolsky et al., 2007). This method is commonly applied in permafrost models (Goodrich, 1978; Nicolsky et al., 2007; Dall' Amicoet al., 2011; Hipp et al., 2012; Langer et al., 2013) and has also recently been applied in a land surface model (Ringeval et al., 2012). Although the method is more physically realistic it requires greater computing resources. This may lead to limitations in the spatial resolution, the length of time that can be modeled, and the number of simulated land surface classes, etc.

Both categories of numerical models have their disadvantages when they are applied for

regional permafrost simulation. Apart from numerical models, analytical solutions also exist that can be used for solving phase change problems. For example, exact Neumann solutions to freezing and thawing problems exist for idealized cases, e.g. for infinite or semi-infinite homogeneous material, steady upper boundary conditions, etc. (Lunardini, 1981). Stefan's equation, which was originally used to predict the thickness of sea ice, is widely used due to its simple form (Lunardini, 1981); an algorithm for applying Stefan's equation to a layered system (e.g. soil) was developed by Jumikis (1977) and applied in a hydrological model by Fox (1992). However, predictions from the Stefan algorithm usually overestimate the depths of freeze/thaw fronts as it neglects any heat transport beneath the front. In order to mitigate this problem of overestimation, Woo et al. (2004) developed a two-directional Stefan algorithm (TDSA). Yi et al. (2009a) integrated a TDSA within a Terrestrial Ecosystem Model (TEM) in order to first simulate the depths of freezing or thawing fronts, and then update the soil temperatures for layers above the uppermost front, beneath the lowermost front, and between these two fronts. This is an efficient method and is able to track the positions of fronts within thick soil layers.

Although models using the above methods to simulate permafrost dynamics over large regions have been validated using *in situ* measurements, few of them have been verified against analytical solutions for both freeze/thaw fronts and soil temperatures at different depths, which is as important for model validation (Romanovsky et al., 1997). Furthermore, conceptual and numerical permafrost landscape models also require suitable upscaling methods ranging from local to global scales, based on field-based knowledge of the surface characteristics, key processes and data collection of key parameters (Boike et al. 2012).

In this study we aimed to develop and test a model that could simulate permafrost dynamics under different types of land surface, i.e. different thicknesses of snow cover, of the organic layer, and of water cover. We first verified our dynamic organic soil version of the TEM (DOS-TEM), which used the TDSA to simulate soil freezing/thawing processes, with analytical solutions for idealized cases. We then modified the model to take into account the effects that water bodies of various sizes have on the thermal dynamics of permafrost and compared the output with *in situ* measurements from Samoylov Island in the Lena Delta, Siberia. Finally, we compared the simulations beneath different land surface types in order to investigate the vulnerability of permafrost to water bodies.

2 Methods

2.1 Site description

Samoylov Island (72°22'N, 126°30'E) is located in the south-central part of the Lena River Delta of Siberia (Figure 1); it covers an area of about 4.3 km^2. The average annual mean air temperature on Samoylov Island from 1998 to 2011 was -12.5°C and the average total summer rainfall 125 mm (Boike et al., 2013). Samoylov Island contains two major geomorphological units: a floodplain, and an elevated Holocene terrace that is characterized by low-centered polygonal tundra. The elevated terrace comprises ~70% of the total area of the island and contains numerous ponds and thermokarst lakes. On average, the land surface of the terrace consists of 58% dry tundra, 17% wet tundra, and 25% water surfaces (Muster et al., 2012). A 26.75 m borehole was drilled in 2006, in an area that consists of about 60% polygon centers and about 40% polygon rims, with a negligible areal proportion of ponds (Figure 1). Further information concerning the climate, permafrost, vegetation, and soil characteristics can be found in Boike et al. (2013).

2.1.1 Meteorological data processing

The collection of meteorological measurements on Samoylov Island started in 1998. The daily mean air temperature, wind speed, vapor pressure, net radiation, downward solar radiation, and total daily precipitation were calculated from hourly measurements. If more than 25% of the measurements were missing in any one day, no value was recorded for that day. If more than 25% of the daily values in a particular month were missing, no value was recorded for that month. We replaced the missing monthly values as follows:

(1) Air temperature and precipitation (snow + rain) measurements for the same month, available from the nearby Stolb meteorological station (which has datasets from 1956, but with large gaps during the 1970s), were used to replace the missing values.

(2) Long term-mean values were used to replace some values for air temperature and precipitation that remained missing after step (1) above, as well as missing values for wind speed, radiation, and vapor pressure. We calculated the long-term monthly mean for air temperature and precipitation between 1981 and 2011 using measurements from the Stolb meteorological station, and for wind speed, downward shortwave radiation, and vapor pressure between 1998 and 2011 using measurements from the Samoylov site.

To illustrate the differences between different datasets, we compared the monthly air temperature and precipitation datasets from Samoylov Island with those from Stolb and the global reanalysis dataset from the Climate Research Unit (CRU TS3.1), available from http://badc.nerc.ac.uk/view/badc.nerc.ac.uk__ATOM__dataent_1256223773328276 (Figure 2).

2.2 Model descriptions

The Terrestrial Ecosystem Model (TEM) family of models is designed to simulate the carbon and nitrogen pools within vegetation and soil, and the carbon and nitrogen fluxes between vegetation, soil, and the atmosphere (McGuire et al., 1992). The most recent TEM version (i.e. the DOS-TEM) can simulate the dynamics of organic soil layers, which can be subject to fire disturbances and to ecological successions (Yi et al., 2010). The DOS-TEM consists of four modules, these being the environmental, ecological, fire disturbance, and dynamic organic soil modules. The environmental module operates on a daily time interval using mean daily air temperature, surface solar radiation, precipitation, and vapor pressure, which are downscaled from monthly input data (Yi et al., 2009a). It takes into account radiation and water fluxes between the atmosphere, canopy, snow pack, and soil. Soil moisture and temperature of all soil layers are updated daily. A two-directional Stefan algorithm is used to predict the depths of freezing or thawing fronts within the soil (Woo et al., 2004); it first simulates the depth of the front in the soil column from the top downward, using soil surface temperature as the driving temperature; it then simulates the front from the bottom upward using the soil temperature at a specified depth beneath a front as the driving temperature (bottom-up forcing). If a layer contains a freezing or thawing front, this layer is then divided into two layers (Figure A1b). The temperatures of soil layers above the uppermost freezing or thawing front and beneath the lowermost freezing or thawing front are updated separately by solving finite difference equations. The thermal properties of soil layers are affected by their water content (Yi et al., 2009a).

2.3 Model modifications

We made three modifications to the DOS-TEM in order to simulate the effects that water bodies (Figure A1a) have on freezing or thawing processes. (1) As shown in Figure A3a, the volumetric water content of a polygon center is not equal to 1, due to the soil surrounding water bodies. We took into account this effect by calculating the volumetric water content of different layers within water bodies of various sizes (Figure A3); details are presented in

Appendix B. (2) When updating the thermal state of water layers they were treated in the same way as soil layers, but with different thermal properties. We followed the model of Hostetler et al. (1990) to calculate the eddy diffusion coefficients for the water layers, which were then used, together with the molecular diffusion coefficient of water, to calculate the heat transfer within the water bodies and the heat exchange with the underlying sediments: details are presented in Appendix B. (3) The original DOS-TEM only simulated bottom-up forcing for the deepest freezing or thawing front. However, taliks probably exist beneath some water bodies, and more than two freezing or thawing fronts may exist at the same time. We therefore implemented top-down and bottom-up forcing separately for each front (Appendix A).

The soil thermal conductivity in the DOS-TEM was initially calculated according to Farouki (1986). However, preliminary testing showed that the resulting soil thermal conductivities were higher than those derived from field measurements (Langer, et al., 2011 a and b). We therefore used the more realistic parameterization according to Johansen (1975) and Côté and Konrad (2005). Further details on the parameterization used are provided in Appendix C.

2.4 Model verification, validation and sensitivity tests

2.4.1 Comparisons with analytical solutions

Three different materials were tested in this study, i.e. water, minerals (sand), and organic soil. The properties of these materials are listed in Table 1. The initial temperature of each material at different depths (up to 5000 m in the DOS-TEM) was set to -10^{o}C, and the temperature at the upper boundary of each material was set to 5^{o}C over the whole simulation period (100 yrs). We assumed zero heat flux conditions at the lower boundary, i.e. at 5000 m depth. The temperatures and the depth of the thawing front obtained from the DOS-TEM were compared with those from analytical solutions and those obtained using the one-directional Stefan's equation. For the DOS-TEM, the temperature at a specific depth was calculated by linear interpolation between the temperatures of overlying and underlying layers. To test the sensitivity of the model to the depth used for the bottom-up forcing, we tried bottom-up forcing at different depths below the thawing front (i.e. at 50 cm, 1 m, 2 m, 5 m, and 20 m). In order to test the effects of total soil/water thickness, we also evaluated the DOS-TEM using different depths for the lower boundary (50, 500, and 5000 m). The maximal thickness of the soil/water layer was set to 1 m, 10 m, and 100 m for runs with the lower boundary at 50 m, 500 m, and 5000 m depth, so that the total number of layers was constant for each run.

2.4.2 Comparisons with *in situ* measurements

Test sites

We tested the DOS-TEM for soil or water temperatures at 4 different sites, i.e. on a polygon rim (*rim*), in a polygon center without standing water (*center*), in a polygon center with standing water (*pond*), and in a larger thermokarst lake (*lake*). These sites are considered to represent the most important types of land surfaces in the polygonal tundra landscape of Samoylov Island. The configurations of water and organic soil characteristics for the different land surface types used in the model are presented in Table 2. We used about 65 m of mineral soils (saturated sand with a porosity of 0.6) in 12 layers. The DOS-TEM assumes bedrock beneath the soil layer (Figure A1a); in each case we used 420 m of bedrock in 5 layers to represent the frozen sediments on Samoylov Island. The ground heat flux at the bottom of the bedrock was set to 0.053 w/m^2 (Pollack et al. 1993).

The simulated soil temperatures for the four different land surface types were compared to temperature measurements from a 27m borehole on Samoylov Island (Boike et al. 2013).

Surface temperatures

The DOS-TEM is not able to simulate the surface temperatures of water, land, or snow. We therefore used linear regression to establish the relationship between measured daily surface temperatures and air temperatures during those periods of 2011in which both temperatures were above 0^{o}C, as follows: for water $T_{surf} = 0.563T_{air} + 4.735$ (coefficient of determination (R^2) = 0.41, number of pairs of data (n) = 84), for land, $T_{surf} = 0.643T_{air} + 2.231$ (R^2 = 0.54, n = 84). For snow, frozen soil and frozen water we assumed $T_{surf} = T_{air}$. A similar method has previously been used in Yi et al. (2013).

Snow cover

Wind drift is an important process that redistributes snow on the polygonal tundra landscape. Field measurements of annual maximum snow thickness show depths of usually 15-40 cm in polygon centers and much less on polygon rims (10-30 cm, with an average of about 15 cm) and frozen lakes (Boike et al., 2013). Zhang et al. (2012) introduced a snow drift factor into their NEST model. The factors for *rims*, *centers*, and water bodies (*ponds* and *lakes*) were 0.5, 0, and -0.25, respectively, with a positive value indicating a loss of snow due to wind drift. However, a preliminary model run indicated that the simulated snow thicknesses were overestimates, for all sites. In this study we therefore identified site-specific threshold values for maximum snow accumulation based on field observations, as follows:

$$D_{snw,max} = \begin{cases} 0.15 & rim \\ \Delta H + 0.15 & centre \\ 0.15 & lake \end{cases}$$

*w*here $D_{snw,max}$ is the maximum snow thickness (m), Δ H is the microtopographic relief (m) (see Figure A3).

Soil and water properties

For the soil thermal properties we used two sets of parameters, one derived from field temperature measurements (Langer et al., 2011a and b) and the other calculated from an algorithm proposed by Luo et al. (2009), details of which can be found in Appendix C (Table 3). For water, we increased the calculated value of the eddy diffusion coefficient by a factor of between 10 and 100 (following Subin et al., 2012), in order to take into account the effects of convection currents caused by complex lake topography and density instability.

Initialization

The *rim*, *center*, and *pond* sites were all initialized using a temperature of -10°C for all water, soil, and bedrock layers; the *lake* site was initiated with -10°C for all soil and bedrock layers and with 0°C for water layers. For the equilibrium run, the model was forced by an average annual cycle that was generated using the monthly averages generated from climate data available for 1981 to 2011. When the difference in annual mean unfrozen soil thickness between two consecutive years was less than 0.01 cm the model was considered to be in a state of equilibrium. The equilibrium run time was set to between 50 and 400 yr. The period from 1981 to 2003 was used for model spin-up, and we compared the simulations with measurements collected after 2003.

2.4.3 Effects of (maximum) water depth

Polygon centers and lakes of various sizes and water depths are distributed across much of Samoylov Island. In order to investigate the effect that the size and water depth of polygon ponds and lakes have on the thickness of the underlying unfrozen soil we ran the DOS-TEM for a shallow, medium, and deep polygon pond (with maximum water depths of 20, 60, and 120 cm), and for a shallow, medium, and deep lake (with maximum water depths of 2, 4, and 6 m). For each polygon pond or lake the model was run with water depths of between 0 and 100% of the maximum water depth, at intervals equal to 5% of the maximum water depth. The annual mean unfrozen soil thickness from 2003 to 2011 was calculated for each run, for comparison purposes.

3 Results

3.1 Comparisons with exact Neumann solutions and Stefan equations

The bottom-up forcing in the DOS-TEM is very important for accurate simulation of the position of the thawing front using Stefan's algorithm (Figure 3). For all cases of water, mineral soil, and organic soil, the thawing fronts simulated without bottom-up forcing were very close to those calculated using Stefan's equation. The root mean squared errors (RMSEs, n = 36,500) between thawing fronts simulated without bottom-up forcing and those from exact Neumann solutions for three different idealized cases were greater than 1.128 m. In contrast, the RMSEs between the thawing fronts simulated with bottom-up forcing and those from exact Neumann solutions were less than 0.047 m (Table 4).

The simulated water or soil temperatures and thawing fronts were not sensitive to the depth of bottom-up forcing (Figure 3). For example, there was almost no difference between the thawing fronts simulated for bottom-up forcing at depths of between 0.5 m and 20 m, in all three cases (water, mineral soil, and organic soil). The differences between thawing front simulations using bottom-up forcing and those from Neumann solutions were also very small (Figure 3). Taking bottom-up forcing at a depth of 1 m beneath the thawing front as an example, most of the RMSEs for temperatures at depths shallower than 1 m were less than 0.01^{o}C, and approximately 0.1^{o}C for depths greater than 1m (Figure 4 and Table 5).

The simulated temperatures were sensitive to the total thicknesses of the various materials, especially that of mineral soil which has the highest thermal conductivity and the lowest water content (Table 4).

3.2 Comparisons with in situ measurements

3.2.1 Snow thicknesses

The simulated snow thickness from the DOS-TEM was greater than 80 cm at all sites for 2005-2006, and decreased thereafter (Figure 5). However, measurements at the *center* site showed that the monthly maximum snow thickness was only 40 cm. After setting a maximum snow thickness, the differences in snow thickness between the 4 sites were similar to field observations, but the inter-annual variability was very small. Since we assumed that snow only accumulates on frozen layers of water or soil, the starting date for snow accumulation at *pond* and *lake* sites was usually later than at *rim* and *center* sites. The simulated starting dates

for snow accumulation in the autumn of 2010 were about one month later than the observed starting dates.

3.2.2 Temperatures of shallow layers

For the *rim* site, soil temperatures for model runs that included snow drift compared well with actual measurements at depths of both 2 cm and 51 cm (Figure 6). The simulated soil temperatures at 51 cm were slightly lower than measured temperatures during summer months. The simulated soil temperatures using the calculated thermal properties (Appendix C) were close to those simulated using the derived thermal properties at 2 cm depth but varied by about 1-3^{o}C at 51 cm depth. The effect of snow was very obvious: where no maximum snow thickness had been set the simulated soil temperatures were up to 10^{o}C warmer than the measured soil temperatures.

For the *center* site, the performance of the DOS-TEM was similar to the *rim* site during the summer seasons (Figure 7). The DOS-TEM overestimated the soil temperatures at 40 cm depth in several of the winters. Using different soil thermal properties did not result in any obvious differences in soil temperature, and setting a maximum snow thickness had less effect than for the *rim* site.

For both *rim* and *center* sites, the simulated soil temperatures fell rapidly during the fall of 2010, possibly due to the later snow fall in the simulation (Figures 5, 6, and 7).

For the *pond* site, the seasonal cycle of simulated water temperature had a reduced amplitude (Figure 8). For example, the simulated water temperature in the lower part of the *pond* site was 20^{o}C warmer than actual measurements from the winter of 2008-2009. As an additional experiment we reduced the maximum snow thickness from 15 cm to 2 cm, which brought the simulated water temperatures in winter down to the measured temperatures. Changing the water eddy diffusion coefficient by a factor of between 10 and 100 did not result in any obvious differences between model runs.

For the *lake* site, the simulated water temperatures in the upper part of the lake were not as sensitive to the eddy diffusion coefficient as those in the lower part of the *lake* (Figure 9). The simulation using the default water eddy diffusion coefficient considerably underestimated the water temperature (by about 10^{o}C) in the lower part of the *lake*. Increasing the eddy diffusion coefficient by a factor of 100 improved the simulation.

In the following two subsections we only analyze the freezing and thawing fronts and the deeper soil temperatures from the *lake* site on the basis of simulations with a maximum snow

thickness, derived soil thermal properties, and an eddy diffusion coefficient increased by a factor of 10.

3.2.3 Freezing and thawing fronts and unfrozen soil thicknesses

The simulated shapes of freezing and thawing fronts at the *rim* and *center* sites were similar from 2003 to 2011 (Figure 10). The thawing fronts did not survive through the winter months and into the following year. However, multiple thawing and freezing fronts were simulated at the pond site. In an additional test performed with 2 cm maximum snow thickness, the soil temperature was colder than it was with 20 cm maximum snow thickness and the shapes of the thawing fronts were different (Figure 10, c) and d)). From 2003 to 2011 the average maximum depth of thawing fronts in soils under water was 0.47 for simulations with 2 cm maximum snow thicknesses and 3.86 m for those with 20 cm maximum snow thickness. The simulated thawing fronts at the *lake* site occurred at an average depth of 12.90 m below the lake floor.

The volumetric water content (VWC) of *centers* or *lakes* was only 6% less (at the most) than the water depths measured on Samoylov Island (Table A1). We investigated the effects of including a VWC calculation by comparing two sets of simulations: one taking into account the effects of water depth on the VWC, and the other using a VWC of 1. The differences of multi-year mean simulated unfrozen soil thickness were very small (less than 1 cm) for the *lake* and *pond* site with 2 cm maximum snow thickness. However, for the *pond* site with 20 cm maximum snow thickness, the simulated unfrozen soil thicknesses for the two simulations were about 1.60 and 3.66 m, respectively.

In order to investigate the effects of eddy diffusivity and equilibrium run time, we performed additional sensitivity tests on the *lake* site, with three different eddy diffusivities (the original value of ke1, and additional values of ke10, and ke100) and 3 equilibrium run times (200, 400, and 600 yr). The simulation with ke1 and a 200 yr equilibrium run time had the smallest talik thickness (8.42 m), while that with ke100 and a 600 yr equilibrium run time had the greatest unfrozen soil thickness (16.11 m). For a particular equilibrium run time, the effect that increasing the eddy diffusivity from ke1 to ke10 had on unfrozen soil thickness was greater than the effect when it was increases from ke10 to ke100. For a particular eddy diffusivity value, the effect of increasing the equilibrium run time from 200 to 400 yr was similar to that of increasing it from 400 to 600 yr (Table 6).

Previous versions of the DOS-TEM only considered top-down forcing for the uppermost front and bottom-up forcing for the lowest front. In this study, we implemented both top-down and bottom-up forcing for each front. There were very small differences at the *rim, center* and *pond* sites, but major differences at the *lake* site. For example, with eddy diffusivity increased by a factor of 10 and a 400 yr equilibrium run time the simulated unfrozen soil thicknesses over the period from 2003 to 2011 was about 12.89 m using our version of the DOS-TEM, compared to 10.96 m using the previous version (Yi et al., 2009a).

3.2.4 Temperatures of deep layers

The averages of the modeled annual mean soil temperatures at 26.75 m depth over the period from 2007 to 2011 were approximately -10.16, -9.14, -99, and -0.61^{o}C for the *rim*, *center*, *pond*, and *lake* sites, respectively (Figure 11). The *centers* and *rims* are typically about 10 m across and horizontal temperature differences due to surface heterogeneities can be assumed to be largely averaged out at depths greater than 10m. The borehole temperatures at depths greater than 10 m therefore represent an average temperature beneath both polygon centers and polygon rims. If the simulated temperatures from the *rim* and *center* sites were averaged by 40% and 60%, respectively, then the overall mean simulated temperature at 26.75 m depth would be -9.55°C, which is about 0.75 °C colder than the temperature recorded in the borehole at the same depth and over the same period of time.

As with the unfrozen soil thicknesses, the soil temperature at 26.75 m depth at the *lake* site was sensitive to changes in eddy diffusivity and equilibrium run time (Table 6).

3.3 Effects of (maximum) water depth

For polygon centers with small maximum water depths (e.g. 20 and 60 cm), increasing water depth caused a slight increase in the multi-year mean (2003-2011) unfrozen soil thickness (Figure 12a). For deep *polygon centers* (e.g. up to 1.2 m), the unfrozen soil thickness started to increase rapidly when the water depth was about 0.8 m and reached a maximum (of about 8.5 m) at a water depth of around 1.05 m, before it decreased again rapidly for water depths greater than 1.05 m. Increasing the water depth in the *lake* also increased the unfrozen sediment thickness; the sensitivity of the simulated unfrozen sediment thickness was particularly high when the *lake* water depth was between 1.0 and 2.0 m (Figure 12b). The unfrozen sediment thickness was relatively constant (at about 13 m) when water depth was greater than 2.0 m. The unfrozen sediment thickness responses were not sensitive to maximum water depths.

4 Discussion

4.1 Performance of the DOS-TEM

The DOS-TEM is able to simulate multiple freezing and thawing fronts simultaneously. For example, there was a year-long thawing front in the sediment and a freezing and a thawing seasonal front in the water of the lake site, and there were multiple freezing and thawing fronts at the *pond* site (Figure 10). The simulated thawing fronts and soil/water temperatures at different depths compared very well with analytical Neumann solutions for all three materials, and the accuracy was not sensitive to the depth of bottom-up forcing (Figures 3 and 4). The simulated soil/water temperatures compared reasonably well with *in situ* measurements from Samoylov Island (Figures 6, 7, 8, and 9).

Modeling studies usually consider thin layers within the uppermost meter of the soil column to depict daily or seasonal soil temperature dynamics, and then thick layers at greater depths to improve computing efficiency (e.g. Oleson et al., 2004), which may result in problems when attempting to simulate the thermal dynamics of talik. The ground layering in the DOS-TEM, including snow, water, soil, and bedrock, follows the same strategy. Unlike other models, the DOS-TEM can track multiple fronts, even within a single layer. The updating of freezing/thawing fronts is based on the Stefan algorithm, which is very efficient. The subsequent updates of temperature in each layer are similar to those of land surface models using the Crank-Nicolson algorithm, which is also an efficient algorithm. The DOS-TEM itself is therefore an efficient model; for example, it takes only about 10 seconds to simulate a period of 100 years.

4.2 Effects of different land cover types

In this study, we have mainly investigated the effects of snow thickness and water depth on soil thermal dynamics for the different land cover types. Snow thickness has a strong impact on the soil/water temperatures during cold seasons. At the *rim* site, differences between simulated soil temperatures with and without taking snow drift into account were usually greater than 10^{o}C (Figure 6). At the *center* site, the simulated snow thickness was greater than the measured thickness (Figure 5) and the simulated soil temperatures were warmer than the measured temperatures (Figure 7). The differences at the *pond* site were even greater (Figure 8).

The timing of snowfall is an additional factor affecting the thermal dynamics of soils. The snowfalls simulated for the fall of 2010 were later than the measured snowfalls (Figure 5), which caused early decreases in soil temperatures at the *rim* and *center* sites (Figures 6 and 7). In the real world, early snowfall might be expected to melt in the unfrozen water of the *pond* and *lake* sites; in the model, snow accumulated only after the first 2 cm of water was frozen. In the fall of 2010 there was therefore no time-lag between the simulated and measured water temperatures (Figures 8 and 9).

Water ponding has a very important influence on the underlying unfrozen soil thickness (Figure 10) and the permafrost temperature (Figure 11). Our sensitivity tests indicate that, under the present climate on Samoylov Island, the unfrozen soil thickness is very sensitive to water depths of between 1 and 2 m for thermokarst lakes, and between 0.8 and 1.2 m for polygon centers. This has significant implications for the development of talik under thermokarst lakes: following the melting of segregated ice under polygonal tundra (and associated surface subsidence) the development of a thermokarst lake or polygon center can accelerate if the water depth in the lake or pond exceeds a certain threshold. Similarly, talik beneath a thermokarst lake can disappear if the water depth in the lake falls below a certain threshold (van Huissteden et al., 2011).

4.3 Limitations and uncertainties

Because of the harsh Arctic environment some measurements of atmospheric variables are not available from Samoylov Island and the missing values were replaced with those from the nearby Stolb meteorological station. Air temperatures from the Stolb station (*T_stolb*) compared very well with those from Samoylov Island (*T_samoylov*): *T_stolb* = 0.97*T_samoylov*+0.65; R^2 = 0.99; n = 80. The growing season precipitation at the Stolb station (*P_stolb*) also compared reasonably well with that for Samoylov Island (*P_stolb* = 0.62*P_samoylov*+8.35; R^2 = 0.53; n = 37), with averages of 26.4 and 29.3 mm/month, respectively. Since there were no precipitation measurements for the cold seasons on Samoylov Island, it is impossible to assess any uncertainty associated with snowfall.

Running ecosystem models for regional or global applications requires large scale reanalysis datasets, such as the global datasets of the Climate Research Unit (CRU), the European Centre for Medium-Range Weather Forecasts (ECMWF), or the National Centers for Environmental Prediction - National Center for Atmospheric Research (NCEP-NCAR). In this study we compared the air temperature and precipitation from the CRU dataset with those

from Samoylov Island. Air temperatures from the CRU were close to those for Samoylov Island in summer, but about 15°C colder in January (Figure 2). The monthly average precipitation in the growing season between 1998 and 2009 was 41.2 mm/month from the CRU and 29.3 mm/month for Samoylov Island. It is clearly important to investigate the uncertainties associated with input data when using models for large scale cold region applications (Clein et al., 2007).

Wind drift is a common process involved in redistributing snow on the heterogeneous landscape of the Arctic tundra (Sturm et al., 2001). There are, however, no measurements of snowfall and snow cover thickness available for the various terrain units of Samoylov Island, making the parameterization of snow drift impossible. Zhang et al. (2012) used snow drift factors and in this study we have set maximal snow thicknesses to simulate the differences in snow thicknesses between different land surface types. However, both methods are very empirical. These measurements will in future need to be collected in situ in order to develop valid parameterizations for snow drift.

The surface temperatures of snow, soil, and water are critical boundary conditions for solving finite difference equations; they are dependent on atmospheric conditions as well as the snow/soil/water conditions (Yi et al., 2013). In models with hourly time steps, snow/soil/water surface temperatures are calculated by iteratively solving the surface energy balance equation for the different surfaces. This involves incoming and reflected solar radiation, incoming and outgoing longwave radiation, sensible and latent heat fluxes between the surface and the atmosphere, and ground heat flux (Oleson et al., 2004). In this study we have used a regression model to calculate surface temperatures on the basis of existing measurements. These algorithms performed better for the *rim* and *center* sites than for the *pond* and *lake* sites.

The exchange of energy in water bodies is not only a result of molecular diffusion and eddy diffusion, but also of other processes such as convection caused by water density instability and complex lake-bottom shapes, which have not been taken into account in this study. We followed Subin et al. (2012) to simulate these effects implicitly by increasing the eddy diffusion coefficient. For example, in order to agree with the dynamics of water temperatures at bottom of the lake (6 m depth) at the *lake* site, the eddy diffusion coefficient had to be increased by at least a factor of 10 (Figure 9). Extensive work is required to test this approach over other lakes in different regions.

Models are commonly run with a multi-year mean climate in order to obtain a state of equilibrium, which should only relate to the climatic and land surface characteristics, and should not be affected by the amount of time used. However, the length of time used for an equilibrium run affects the simulated unfrozen soil thickness of polygon centers and lakes when the water body depth exceeds a threshold value. For example, it took less than 100 years for the DOS-TEM to reach equilibrium at the *rim* and *center* sites but it never reached equilibrium at the *lake* site, even after 600 years. It is therefore important to have actual measurements of talik thicknesses beneath water bodies in order to determine the number of years required for an equilibrium run and to validate model outputs. Unfortunately, however, such information is not readily available at present. A new technology known as surface nuclear magnetic resonance has recently been used over thermokarst lakes to measure the underlying talik thickness (Parsekian et al., 2013), and promises to provide useful information on talik that can be used to improve modeling in future studies.

Lateral heat gradients clearly exist beneath the different land surface types of the polygonal tundra (Figure 11), but since the DOS-TEM is a one-dimensional model it is unable to simulate lateral heat exchange. A 2- or 3-dimensional model would be better able to simulate the thermal processes in complex Arctic tundra landscapes (e.g., Ling and Zhang, 2003; Plug and West, 2009; van Huissteden et al., 2011; Kessler et al., 2012), but such models are difficult to apply over large regions.

Thermal processes vary under the different land surfaces of the heterogeneous polygonal tundra. For example, talik was present under the *lake* site, but not under the *center* or *pond* sites. In our study we have assumed fixed shapes for polygon centers and lakes, but in future studies it would be desirable to include the dynamics of thermokarst lake development.

4.4 Outlook

Land surfaces are heterogeneous at various spatial scales and land surface models (LSMs) with coarse resolutions (usually hundreds of kilometers) use different technologies to take this heterogeneity into account. Early LSMs only considered the major land surface type within each grid cell (Manabe, 1969); parameters of different land surface types were subsequently aggregated for each grid (Arain et al., 1999). With recent advances in computing power and remote sensing technology, it has become possible to explicitly consider different types of land surface, such as those with different plant function types, urban areas, water, etc. (Oleson et al., 2004). Our study has indicated that the heterogeneity of Arctic polygonal tundra results

in marked differences in soil thermal dynamics (Figure 10 and 11). In order to simulate methane emissions from polygonal tundra ecosystems on a regional scale it is therefore crucial to distinguish between polygon rims, polygon centers (with varying water levels), and thermokarst lakes at different stages of development. The sensitivity analysis suggests that it is necessary to, at the very least, consider polygon rims, polygon centers (with maximum water depths of less than 0.8 m and with several water depths between 0.8 and 1.2 m), and lakes. The following steps can be used to obtain regional input for the above-mentioned classes:

1) The proportion of surface water over regions of polygonal tundra ecosystem can be retrieved from remote sensing albedo datasets (Muster et al., 2013) and the maximal proportion of surface water over different periods.

2) The distribution of the area covered by polygon centers can be established following Cresto Aleina et al. (2012).

3) The relationship between water area and water depth can be established on the basis of in situ measurement data (Wischnewski, 2013).

5 Conclusions

In this study we have modified an ecosystem model to simulate thermal processes under the different land surface types of a polygonal tundra landscape on Samoylov Island, in the Lena Delta of Siberia. The simulated freeze-thaw dynamics and soil/water temperatures compared very well with analytical Neumann solutions for three different materials in idealized runs. Despite a number of limitations and uncertainties relating to model parameterization and data input, the simulated soil/water temperatures compared reasonable well with *in situ* measurements. The modified model is thus very efficient and suitable for large-scale regional applications.

Microtopographic relief has an important effect on snow and water cover, which in turn exert important influences on the different thermal processes that operate under the various land surface types. Sensitivity tests have indicated that thermal processes are very sensitive to changes in water depth when the depth is between approximately 1 and 2 m for lakes, and between 0.8 and 1.2 m for polygon center. The different land surface types of polygonal tundra ecosystems need to be taken into account in large scale ecosystem models, as well as water dynamics, in order to be able to accurately simulate methane emissions.

Appendix A. Updating fronts and temperatures

The updating of temperatures of snow/water/soil/rock layers involves two steps: 1) updating freezing/thawing fronts using the two-directional Stefan algorithm (TDSA) method, and 2) updating temperatures by solving finite difference equations.

The TDSA is based on a well-established Stefan algorithm for determining the positions of freezing/thawing fronts in layered systems (Jumikis, 1977). The TDSA first updates fronts from top-down, and then from bottom-up. In this way it is able to overcome the problem of overestimating of front positions (Woo et al., 2004). A detailed description of the calculation of the positions of freezing/thawing fronts has been presented in Woo et al. (2004), and in Appendix E1 of Yi et al. (2009). Herein we describe only the changes made to the TDSA.

For coexisting multiple fronts, previous versions of the TDSA only calculated the downward movement of the uppermost front using the surface soil temperature as forcing temperature, and the upward movement of the lowest front using the temperature of a specified layer as forcing temperature from bottom. The temperatures between two fronts are assumed to be close to 0^{o}C. This assumption might not be valid for thermokarst lakes, which usually have a year-long thawing front in the sediment. In this study we implemented top and bottom forcing temperatures for each front. The top-down forcing temperature at a specified distance (1 m in this study) above a front is determined first as shown in Figure A2, which is then used to update the front. Calculations for the bottom-up forcing temperatures are similar to those for top-down forcing temperatures. The energy used for phase changes during the updating of front positions was recorded for each front.

After the freezing/thawing fronts have been updated, the temperature of each layer is updated by solving several sets of finite difference equations using the Crank-Nicholson scheme (see Oleson et al., 2004). The number of sets of equations is determined by number of freezing/thawing fronts. If no front exists then only one set of equations is solved. If one front exists then two sets of equations are solved, one for the layers above the layer with the front and the part layer above the front, and the other for the layers below the layer with front and the part layer below the front. If more than two fronts exist, then three sets of equations are solved: the first set for the layers above the layer with the uppermost front and the part layer above the uppermost front, the second set for the layers below the layer with the lowest front and the part layer below the lowest front, and the third equation for the rest of the layers between the uppermost and lowest fronts. The phase change energy determined during front

updating is used as a source term in the equations. Additional information concerning temperature updating can be found in Appendix E2 of Yi et al., (2009).

Appendix B: Modeling the effects of water

The low-centered polygon landscape of the Arctic tundra can be simplified into polygon rims, polygon centers of various sizes (with and without water), and lakes of various sizes. On the basis of the original soil and snow structure of the DOS-TEM (the previous version of the DOS-TEM had no water), we modeled water bodies above soil layers (Figure A1a) to simulate the effects that the water in polygon centers and lakes has on freezing or thawing dynamics in the underlying soils or sediments. The division of water into layers was the same as that for soils, i.e. 2 cm, 4 cm, 8 cm, …, 2^n cm, where n is the layer index.

Effects of slope on volumetric water content

The slope between a polygon center and its rim (and also between a lake floor and its shoreline) was set to 28^o in our model (Figure A3), on the basis of field observations. The vertical distance between the bottom of a polygon center (or of a lake) and the top of its rim was taken to be the maximum water depth (WD_{max}). We assumed the shape of polygon center (or lake) to resemble part of an inverted cone, with a radius of r_{bot} at the bottom and of r_{top} at the top.

The volumetric water content (*vwc*) of a water layer *i* can then be expressed as:

$$vwc_i = \frac{V_{top,i} - V_{bot,i}}{V_{cyl}} + \frac{V_{cyl} - (V_{top,i} - V_{bot,i})}{V_{cyl}}\theta$$

where

$$V_{top,i} = \frac{1}{3}\pi {r_{top,i}}^2 (dx_i + h)$$

$$V_{bot,i} = \frac{1}{3}\pi {r_{bot,i}}^2 h$$

$$V_{cyl} = \pi {r_{top}}^2 dx_i$$

$$h = \frac{r_{bot,i}}{\tan(\pi \frac{28}{180})}$$

$$r_{bot} = r_{top} - WD_{max} \tan(\pi \frac{28}{180})$$

In these equations $r_{top,i}$ and $r_{bot,i}$ are the top and bottom radii of layer i, dx_i is the thickness of layer i, h is the vertical distance from the top of the cone to the plane with a radius of $r_{bot,i}$, and θ (= 0.6 in this study) is the volumetric water content of the soil rim around the water layers. Field survey results from Samoylov Island indicate that $WD_{max} = 173.1\ln(r_{top}) - 231.45$ (R^2 = 0.99, n = 12; Wischnewski, 2013). In Table A1 we present examples for a small polygon, a large polygon, and a lake.

Thermal dynamics in water

The exchange of energy within water is affected by several processes including molecular diffusion, wind-driven eddy diffusion, buoyant convection, among others. In the DOS-TEM we took into account molecular diffusion, eddy diffusion (which is usually 2-3 orders greater than molecular diffusion: Subin et al., 2012), and other processes, by increasing the eddy diffusion coefficient by a factor of between 10 and 100. In cold seasons with snow and ice cover, the dissipation of energy to the atmosphere would only be realized by molecular diffusion, while in warm seasons and with open water the exchange of energy within the water would be much greater. The seasonal variation in energy exchange coefficients is therefore an important factor in the development of unfrozen soil beneath water bodies. Water layers were treated in the same way as soil and snow layers but with different thermal properties (Figure A1a) when calculating the positions of freezing or thawing fronts and the temperatures within water bodies. Following Hostetler and Bartlein (1990), the governing equation for the one-dimensional model is:

$$C\frac{\partial T}{\partial t} = \frac{\partial}{\partial z}\left((\lambda + CK)\frac{\partial T}{\partial z}\right) + \frac{\partial \Phi}{\partial z}$$

where T is the water/soil/snow temperature (K), t is the time (s), z is the depth from water surface (m), C is the volumetric heat capacity (J/(m^{3}K)), λ is the thermal conductivity of water/soil/snow (J/mKs), K is the conductivity due to eddy diffusion (for water only, J/(mKs)), and Φ is a heat source term (w/m^2). The detailed parameterization of K and Φ can be found in Hostetler and Bartlein (1990).

Appendix C: Soil thermal conductivity

In this study, we applied a soil thermal conductivity scheme proposed by Luo et al., (2009), which integrated the schemes of Johansen (1975) and Côté and Konrad (2005), as follows:

$$k = \begin{cases} K_e k_{sat} + (1 - K_e) k_{dry} & S_r > 1 \times 10^{-5} \\ k_{dry} & S_r \le 1 \times 10^{-5} \end{cases}$$

$$k_{\text{sat}} = \begin{cases} k_s^{1-\theta_{sat}} k_{liq}^{\theta_{sat}} & T \ge T_f \\ k_s^{1-\theta_{sat}} k_{liq}^{\theta_{sat}} k_{ice}^{\theta_{sat}-\theta_{liq}} & T < T_f \end{cases}$$

$$k_s = k_q^q k_o^{1-q}$$

$$k_{dry} = \chi \times 10^{-\eta \theta_{sat}}$$

$$K_e = \frac{\kappa S_r}{1 + (\kappa - 1) S_r}$$

where k, k_{sat}, k_{dry}, k_s, k_{liq}, k_{ice}, k_q, and k_o are thermal conductivities (W/(mK)) of soil, saturated soil, dry soil, soil solid, unfrozen(liquid) water, ice, quartz sand, and other components, respectively. θ_{sat} and θ_{liq} are the porosity and the liquid water content of soil (%), respectively. K_e is the Kersten number. S_r is the soil saturation. χ, η, and κ are 3 parameters whose values for different soil types can be found in Côté and Konrad (2005).

Acknowledgements

This study was supported through grants provided as part of the National Basic Research Program (973 Programme) (2013CBA01807 and 2010CB951402), the Strategic Priority Research Program (XDB030303), and the One Hundred People Plan (O927581001) of the Chinese Academy of Sciences. We are grateful to the German Academic Exchange Service (DAAD) for providing support for the first author to visit Germany. This work was also supported by the European Union FP7-ENV PAGE21 project (contract number 9 GA282700).

References

Abnizova, A., Siemens, J., Langer, M. and Boike, J.: Small ponds with major impact: The relevance of ponds and lakes in permafrost landscapes to carbon dioxide emissions, Global Biogeochem. Cy., 26, GB2041, doi: 10.1029/2011GB004237, 2012.

Arain, A. M., Burke, J. E., Yang, Z.-L., and Shuttleworth, J. W.: Implementing surface parameter aggregation rules in the CCM3 global climate model: regional responses at the land surface, Hydrol. Earth Syst. Sci., 3, 463-476, 1999.

Boike, J., B. Kattenstroth, K. Abramova, N. Bornemann, A. Chetverova, I. Fedorova, K. Frob, M. Grigoriev, M. Gruber, L. Kutzbach, M. Langer, M. Minke, S. Muster, K. Piel, E.-M. Pfeiffer, G. Stoof, S. Westermann, K. Wischnewski, C. Wille, and H. W. Hubberten: Baseline characteristics of climate, permafrost, and land cover from a new permafrost observatory in the Lena River Delta, Siberia (1998 - 2011), Biogeosciences, 10, 2105-2128, 2013.

Boike, J., Langer, M., Lantuit, H., Muster, S., Roth, K., Sachs, T., Overduin, P., Westermann, S. & McGuire, A. D. : Permafrost–physical aspects, carbon cycling, databases and uncertainties. In *Recarbonization of the Biosphere* (pp. 159-185). Springer Netherlands, 2012.

Brown, J., Ferrians Jr., O. J., Heginbottom, J., and Melnikov, E.: Circum-Arctic map of permafrost and ground-ice conditions, National Snow and Ice Data Center/World Data Center for Glaciology, Boulder, CO, 1998.

Clein, J. S., McGuire, A. D., Euskirchen, E. S., and Calef, M. P.: The effects of different climate input datasets on simulated carbon dynamics in the Western Arctic, Earth Interactions, 11, doi:10.1175/EI229.1, 2007.

Côté, J. and J. Konrad: A generalized thermal conductivity model for soils and construction materials, Can. Geotech. J. 42, 443-458, 2005.

Cresto Aleina, F., Brovkin, V., Muster, S., Boike, J., Kutzbach, L., Sachs, T., and Zuyev, S.: A stochastic model for the polygonal tundra based on Poisson-Voronoi Diagrams, Earth Syst. Dynam. Discuss., 3, 453-483, doi:10.5194/esdd-3-453-2012, 2012.

Dall' Amico, M., Endrizzi, S., Gruber, S., and. Rigon, R.: A robust and energy-conserving model of freezing variably-saturated soil, The Cryosphere, 5, 469-484, 2011.

Etzelmüller, B., and Frauenfeld, R.: Factors controlling the distribution of mountain permafrost in the northern hemisphere and their influence on sediment transfer, Arct. Alp. Res., 41, 48-58, 2009.

Farouki, O. T.:Thermal properties of soils, Cold Reg. Res. and Eng. Lab., Hanover, N. H, 1986.

Fox, J. D.: Incorporating Freeze-Thaw Calculations into a water balance model, Water Resour. Res., 28(9), 2229-2244, 1992.

French, H.: ThePeriglacial Environment, 3rd, John Wiley & Sons, Ltd, 2007.

Goodrich, E. L.: Efficient Numerical Technique for one-dimensional Thermal Problems with phase change, Int. J. Heat Mass Transfer, 21, 615-621, 1978.

Hipp, T., Etzelmüller, B., Farbrot, H., Schuler, T. V., and Westermann, S.: Modeling borehole temperatures in Southern Norway - insights into permafrost dynamics during the 20th and 21st century, The Cryosphere, 6, 553-571, 2012.

Hostetler, S. W., and Bartlein, P. J.: Simulation of Lake Evaporation with Application to Modeling Lake Level Variations of Harney-Malheur Lake, Oregon, Water Resour. Res., 26, 2603-2612, 1990.

Johansen, O.: Thermal conductivity of soils, Ph. D. thesis, University of Trondheim, 1975.

Jumikis, A. R.: Thermal Geotechnics, 375 pp., Rutgers Univ. Press,New Brunswick, N. J., 1977.

Kessler, M. A., Plug, L. J., and Walter, K. M.: Simulating the decadal- to millennial-scale dynamics of morphology and sequestered carbon mobilizaion of two thermokarst lakes in NW Alaska, J. Geophys. Res., 117, G00M06, doi:10.1029/2011JG001796, 2012.

Langer, M., Westermann, S., Muster, S., Piel, K., and Boike, J.: The surface energy balance of a polygonal tundra site in northern Siberia - Part 1: Spring to fall, The Cryosphere, 5, 151-171, 2011a.

Langer, M., Westermann, S., Muster, S., Piel, K., and Boike, J.: The surface energy balance of a polygonal tundra site in northern Siberia - Part 2: Winter, The Cryosphere, 5, 509-524, 2011b.

Langer, M**.**, Westermann, S., Heikenfeld, M., Dorn, W., and Boike, J.: Satellite-based modeling of permafrost temperatures in a tundra lowland landscape, Remote Sensing of Environment, 135, 12-24, 2013.

Lawrence, D. M., and Slater, A. G.: Incorporating organic soil into a global climate model, Clim. Dyn., 30, 145-160, 2008.

Ling, F., and Zhang, T.: Numerical simulation of permafrost thermal regime and talik development under shallow thaw lakes on the Alaskan Arctic Coastal Plain, J. Geophys. Res., 108, 4511, doi:10.1029/2002JD003014, 2003.

Lunardini V. J.: Heat transfer in cold climates. Van Nostrand Reinhold: New York, 1981.

Luo, S., Lv, S., Zhang, Y., Hu, Z., Ma, Y., Li, S., and Shang, L.: Soil thermal conductivity parameterization establishment and application in numerical model of central Tibetan Plateau, Chinese Journal of Geophysics, 52, 919-928, 2009. (in Chinese with English Abstract)

Manabe, S.: Climate and the ocean circulation: I. the atmospheric circulation and the hydrology of the Earth's surface, Mon. Weather Rev., 97, 739-774, 1969.

McGuire, A. D., J. Melillo, E. G. Jobbagy, D. Kicklighter, A. L. Grace, B. Moore, and Vorosmarty, C. J.: Interactions Between Carbon and Nitrogen Dynamics in Estimating Net Primary Productivity for Potential Vegetation in North America, Global Biogeochem. Cy., 6(2), 101-124, 1992.

McGuire, A. D., Anderson, L. G., Christensen, T. R., Dallimore, S., Guo, L., Hayes, D. J., Heimann, M., Lorenson, T. D., MacDonald, R. W., and Roulet, N. T.: Sensitivity of the carbon cycle in the Arctic to climate change, Ecological Monographs, 79(4), 523-555, 2009.

Muster, S., Langer, M., Heim, B., Westermann, S., and Boike, J.: Subpixel heterogeneity of ice-wedge polygonal tundra: a multi-scale analysis of land cover and evapotranspiration in the Lena River Delta, Siberia, Tellus B., 64, 17301, doi:10.3402/tellusb.v64i0.17301, 2012.

Muster, S., Heim, B., Abnizova, A. and Boike, J.: Water body distributions across scales: A remote sensing based comparison of three arctic tundra wetlands. Remote Sens., 5, 1498-1523, 2013.

NASA Landsat Program: Lena Delta in Landsat 7/ETM+, Visible Earth, v1 ID: 407 18024, available at: http://visibleearth.nasa.gov/, access: 10 October 2011, 2000.

Nicolsky, D. J., Romanovsky, V. E., Alexeev, V. A., and Lawrence, D. M.: Improved modeling of permafrost dynamics in a GCM land-surface scheme, Geophys. Res. Lett., 34, L08501, doi:10.1029/2007GL029525, 2007.

Oleson, K. W., Dai, Y., Bonan, G. B., Bosilovich, M. G., Dickinson, R. E., Dirmeyer, P., Hoffman, F., Houser, P. R., Levis, S., Niu, G.-Y., Thornton, P., Vertenstein, M., Yang, Z.-L., and Zeng, X.: Technical description of the Community Land Model(CLM), Tech. Rep., NCAR/TN-461+STR, Natl. Cent. for Atmos. Res., Boulder, Colo., 2004.

Parsekian, A. D., Grosse, G., Walbrecker, J. O., Muller-Petke, M., Keating, K., Liu, L., Jones, B. M., and Knight, R.: Detecting unfrozen sediments below thermokarst lakes with surface nuclear magnetic resonance, Geophys. Res. Lett., 40, 535-540, 2013.

Plug, L. J., and West, J. J.: Thaw lake expansion in a two-dimensional coupled model of heat transfer, thaw subsidence, and mass movement, J. Geophys. Res., 114, F01002, doi:10.1029/2006JF000740, 2009.

Pollack, H., Hurter, S., and Johnson, J.: Heat flow from the Earth's interior: Analysis of the global data set. Reviews of Geophysics, 31(3), 267–280, 1993.

Ringeval, B., Decharme, B., Piao, S., Ciais, P., Papa, P., Noblet- Ducoudré, N., Prigent, C., Friedlingstein, P., Gouttevin, I., and Koven, C.: Modelling sub-grid wetland in the ORCHIDEE global land surface model: evaluation against river discharges and remotely sensed data, Geosci. Model Dev., 5, 941-962, 2012.

Riseborough, D. W., Shiklomanov, N. I., Etzelmüller, B., Gruber, S., and Marchenko, S.: Recent Advances in Permafrost Modelling, Permafrost Periglac., 19, 137-156, 2008.

Romanovsky, V. E., and Osterkamp, T. E.: Thawing of the Active Layer on the Coastal Plain of the Alaskan Arctic, Permafrost Periglac., 8, 1-22, 1997.

Sturm, M., McFadden, J. P., Liston, G. E., Chapin, S. F., Racine, C., and Holmgren, J.: Snow-Shrub Interactions in Arctic Tundra: A Hypothesis with Climatic Implications, J. Climate, 14, 336-344, 2001.

Subin, Z. M., Riley, W. J., and Mironov, D.: An improved lake model for climate simulations: Model structure, evalution, and sensitivity analyses in CESM1, Journal of Advances in Modeling Earth Systems, 4, M02001, doi:10.1029/2011MS000072, 2012.

van Huissteden, J., C. Berrittella, F. J. Parmentier, Y. Mi, T. C. Maximov, and A. J. Dolman (2011), Methane emissions from permafrost thaw lakes limited by lake drainage, Nature Climate Change, 1, 119-123.

von Deimling, T. S., Meinshausen, M., Levermann, A., Huber, V., Frieler, K., Lawrence, D. M., and Brovkin, V.: Estimating the near-surface permafrost-carbon feedback on global warming, Biogeosciences, 9, 649-665, 2012.

Wania, R., Ross, I., and Prentice, C. I.: Integrating peatlands and permafrost into a dynamic global vegetation model: 1. Evaluation and sensitivity of physical land surface processes, Global Biogeochem. Cy., 23, GB3014, doi:10.1029/2008GB003412, 2009.

Wischnewski, K.: Temperature Simulation Model for Small Water Bodies in the Arctic Tundra, Lena River Delta (Siberia, Russia), Master thesis, Swiss Federal Institute of Technology Zurich. http://epic.awi.de/32775/, 2013.

Woo, M.-K., Arain, A. M., Mollinga, M., and Yi, S.: A two-directional freeze and thaw algorithm for hydrologic and land surface modelling, Geophys. Res. Lett., 31, L12501, doi:10.1029/2004GL019475, 2004.

Yi, S., Arain, A. M., and Woo, M.-K.: Modifications of a land surface scheme for improved simulation of ground freeze-thaw in northern environments, Geophys. Res. Lett., 33, L13501, doi:10.1029/2006GL026340, 2006.

Yi, S., Woo, M.-K., and Arain, A. M.: Impacts of peat and vegetation on permafrost degradation under climate warming, Geophys. Res. Lett., 34, L16504, doi:10.1029/2007/GL030550, 2007.

Yi, S., McGuire, A. D., Harden, J., Kasischke, E., Manies, K. L., Hinzman, L. D., Liljedahl, A., Randerson, J. T., Liu, H., Romanovsky, V. E., Marchenko, S., and Kim, Y.: Interactions between soil thermal and hydrological dynamics in the response of Alaska ecosystems to fire disturbance , J. Geophys. Res., 114, G02015, doi:10.1029/2008JG000841, 2009a.

Yi, S., Manies, K. L., Harden, J., and McGuire, A. D.: The characteristics of organic soil in black spruce forests: Implications for the application of land surface and ecosystem models in cold regions, Geophys. Res. Lett., 36, L05501, doi:10.1029/2008GL037014, 2009b.

Yi, S., McGuire, A. D., Kasischke, E., Harden, J., Manies, K. L., Mack, M., and Turetsky, M. R.: A Dynamic organic soil biogeochemical model for simulating the effects of wildfire on soil environmental conditions and carbon dynamics of black spruce forests, J. Geophys. Res., 115, G04015, doi:10.1029/2010JG001302, 2010.

Yi. S., Li, N., Xiang, B., Ye, B. and McGuire, A.D.: Representing the effects of alpine grassland vegetation cover on the simulation of soil thermal dynamics by ecosystem models applied to the Qinghai-Tibetan Plateau, J. Geophys. Res., 118, 1-14, doi: 10.1002/jgrg.20093, 2013.

Zhang, Y., Chen, W., and Cihlar, J.: A process-based model for quantifying the impact of climate change on permafrost thermal regimes, J. Geophys. Res.-Atmos., 108(D22), 4695, doi:10.1029/2002JD003354, 2003.

Zhang, Y., Chen, W., and Riseborough, D. W.: Disequilibrium response of permafrost thaw to climate warming in Canada over 1850-2100, Geophys. Res. Lett., 35, L02502, doi:10.1029/2007GL032117, 2008.

Zhang, Y., Sachs, T., Li, C., and Boike, J.: Upscaling methane fluxes from closed chambers to eddy covariance based on a permafrost biogeochemistry integrated model, Global Change Biol., 18, 1428-1440, 2012.

Zhuang, Q., Romanovsky, V. E., and McGuire, A. D.: Incorporation of a permafrost model into a large-scale ecosystem model: Evaluation of temporal and spatial scaling issues in simulating soil thermal dynamics, J. Geophys. Res., 106(D24), 33649-33670, 2001.

Zhuang, Q., Melillo, J., Sarofim, M. C., Kicklighter, D., McGuire, A. D., Felzer, B. S., Sokolov, A., Prinn, R. G., Steudler, P. A., and Hu, S.: CO2 and CH4 exchanges between land ecosystems and the atmosphere in northern high latitudes over the 21st century, Geophys. Res. Lett., 33, L17403, doi:10.1029/2006GL026972, 2006.

Table 1. The thermal conductivity, volumetric heat capacity, volumetric water content, and porosity used in idealized runs for water, mineral soils, and organic soils.

	Thermal conductivity (J/mKs)		Volumetric Heat capacity (10^6 J/m3)		Volumetric water content (%)	Porosity (%)
	Frozen	Unfrozen	Frozen	Unfrozen		
Water	2.29	0.6	2.12	4.19	100	100
Mineral	2.69	1.71	2.06	2.79	33.28	39
Organic	0.37	0.21	0.99	1.84	36.25	90

Table 2. Water and organic soil configurations used in the model for the different test sites.

	Maximum water depth (m)	Water depth (m)	Organic soil
rim	N.A.	N.A.	3 cm moss (dry organic, porosity (p) = 0.95, volumetric water content (vwc) = 0.3) 20 cm organic rich soil (wet organic, p = 0.9, vwc = 0.7)
center	0.25	0	1 m organic soil (saturated organic, p = 0.9, vwc = 0.9)
pond	1.1	1.05	As for center
lake	6	6	As for center

Table 3. Thermal properties of different types of soil on Samoylov Island. The first is derived using soil temperature measurements; the second is calculated using the default scheme in the DOS-TEM.

	Thermal conductivity (W/mK)		Volumetric Heat capacity (MJ/m^3K)		Thermal diffusivity (10^{-6} m^2/s)	
	Unfrozen	Frozen	Unfrozen	Frozen	Unfrozen	Frozen
Dry organic	0.14/0.17	0.46/0.29	0.9/1.43	0.7/0.75	0.30/0.59	0.66/0.39
Wet organic	0.6/0.30	0.95/0.57	3.4/2.6	1.8/1.44	0.18/0.12	0.53/0.40
Saturated organic	0.72/0.54	1.92/1.83	3.8/4.02	2.0/2.16	0.19/0.13	0.96/0.95
Mineral	N.A./1.00	1.9/2.12	N.A./3.16	2.0/2.04	N.A./0.32	0.95/1.03

Table 4. The root mean squared error (n = 36,500) between the thawing fronts (m) from exact Neumann solutions and simulated thawing fronts from the DOS-TEM, with different combinations of total thickness (50, 500, and 5000 m) and bottom-up forcing (b1m: bottom-up forcing at 1 m below front; nobot: no bottom-up forcing) for different materials.

	5000m, b1m	5000m, nobot	500m, b1m	50m, b1m
Water	0.004	1.253	0.032	0.274
Mineral	0.062	4.645	0.177	1.899
Organic	0.012	1.128	0.047	0.065

Table 5. The root mean squared error (n = 36,500) between the temperatures (^{o}C) from exact Neumann solutions and simulated temperatures from the DOS-TEM for different materials, with 5000 m total thickness and bottom-up forcing at 1 m below the thawing front, at depths of between 0.05 and 20 m.

	0.05	0.1	0.5	1	3	6	9	15	20
Water	0.018	0.017	0.044	0.054	0.039	0.039	0.041	0.087	0.071
Mineral	0.011	0.018	0.014	0.010	0.016	0.027	0.030	0.057	0.062
Organic	0.019	0.016	0.009	0.009	0.024	0.042	0.047	0.111	0.110

Table 6. The simulated multi-year mean (2003-2011) unfrozen soil thicknesses (m)/soil temperature (oC) for 26.75 m depth at the lake site using different combinations of eddy diffusivities (ke; 1, 10, and 100 indicate the multiplication factor applied to the original value) and equilibrium run time.

	ke1	ke10	ke100
200 yr	8.42/-1.14	9.94/-1.07	10.56/-1.03
400 yr	11.56/-0.67	12.89/-0.61	13.24/-0.59
600 yr	13.71/-0.40	15.72/-0.34	16.11/-0.32

Table A1. The area, top radius (r_{top}), bottom radius (r_{bot}), maximum water depth (WD_{max}) of polygons or lakes, and their volumetric water contents (vwc) at the top and bottom.

	Area (m^2)	r_{top} (m)	r_{bot} (m)	WD_{max} (m)	VWC	
					Top layer	Bottom layer
Small polygon	50*	3.99	3.95	0.08	1	0.99
Large polygon	200$	7.98	7.30	1.28	1	0.94
Lake	39541&	112.19	109.07	5.86	1	0.98

* Mean average surface area of the smallest polygon centers on Samoylov Island (Wischnewski, 2013);

$ Mean average surface area of the largest polygon centers surveyed on Samoylov Island;

& Area of the large thermokarst lake on Samoylov Island.

Figure 1. (a) Circumpolar permafrost distribution (Brown et al., 1998) and the Lena River Delta, (b) Location of the Samoylov study site within the Lena River Delta, Eastern Siberia (NASA, 2000), and (c) measurement locations on Samoylov Island.

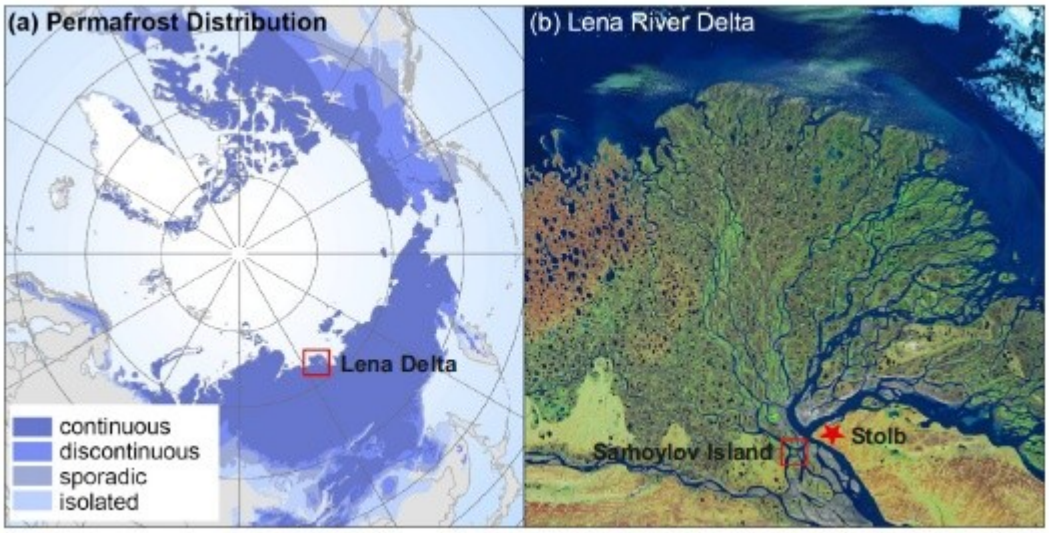

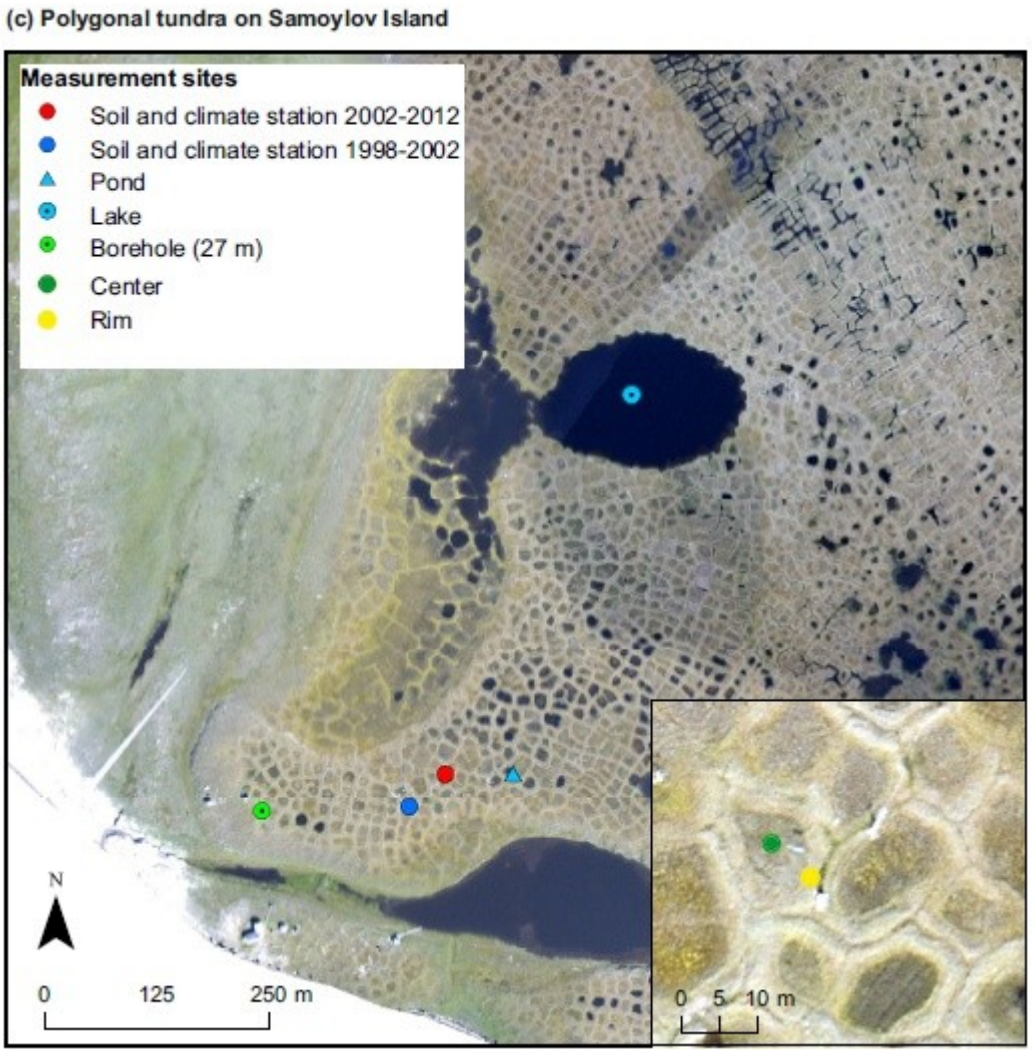

Figure 2. Monthly air temperature (Ta) and precipitation (P) measurements from Samoylov Island (Samoylov), Stolb meteorological station (Stolb), and from the Climate Research Unit global dataset (CRU)

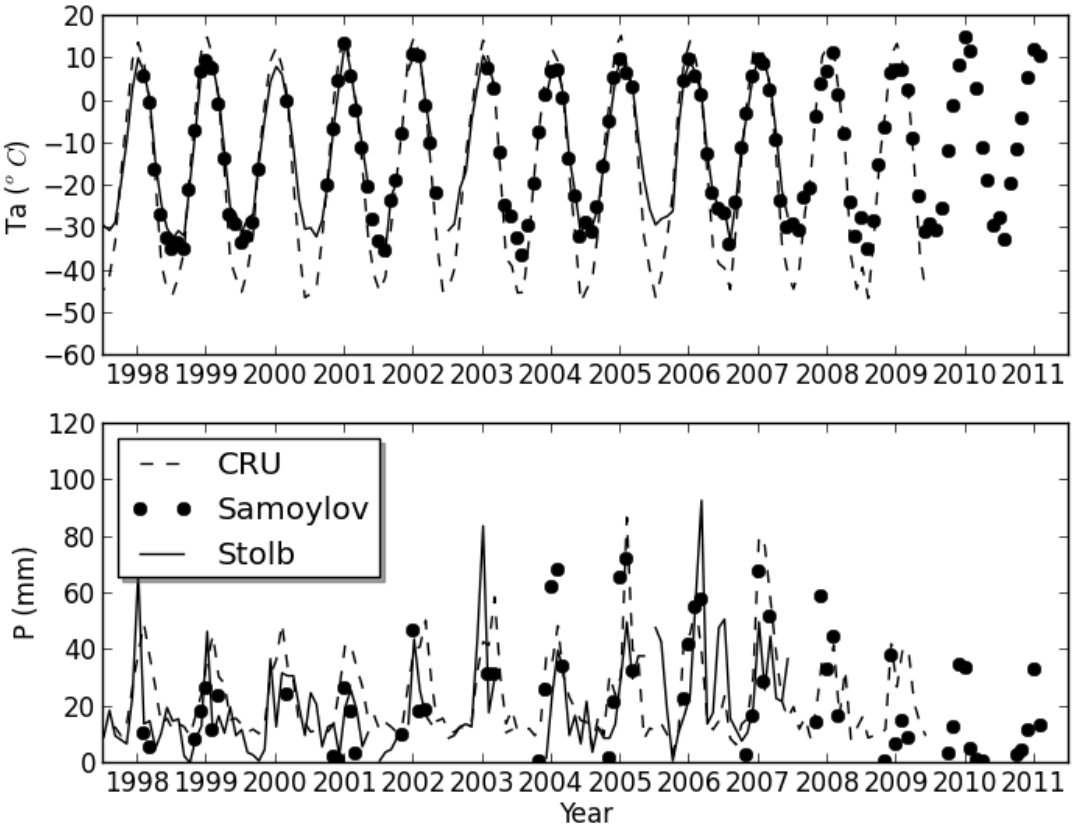

Figure 3. Comparisons of outputs from DOS-TEM simulations, exact Neumann solutions (Exact), and Stefan's equation (Stefan) for a) water, b) mineral soil, and c) organic soil over a one hundred year period. The term B50CM means simulations from the DOS-TEM with bottom-up forcing at 50 cm beneath the lowest freezing or thawing front, and likewise for other similar terms. NOBOT means no bottom-up forcing. The outputs from the DOS-TEM have been plotted for the middle of every tenth year and different cases have been started from different years in order to make the figures more readable.

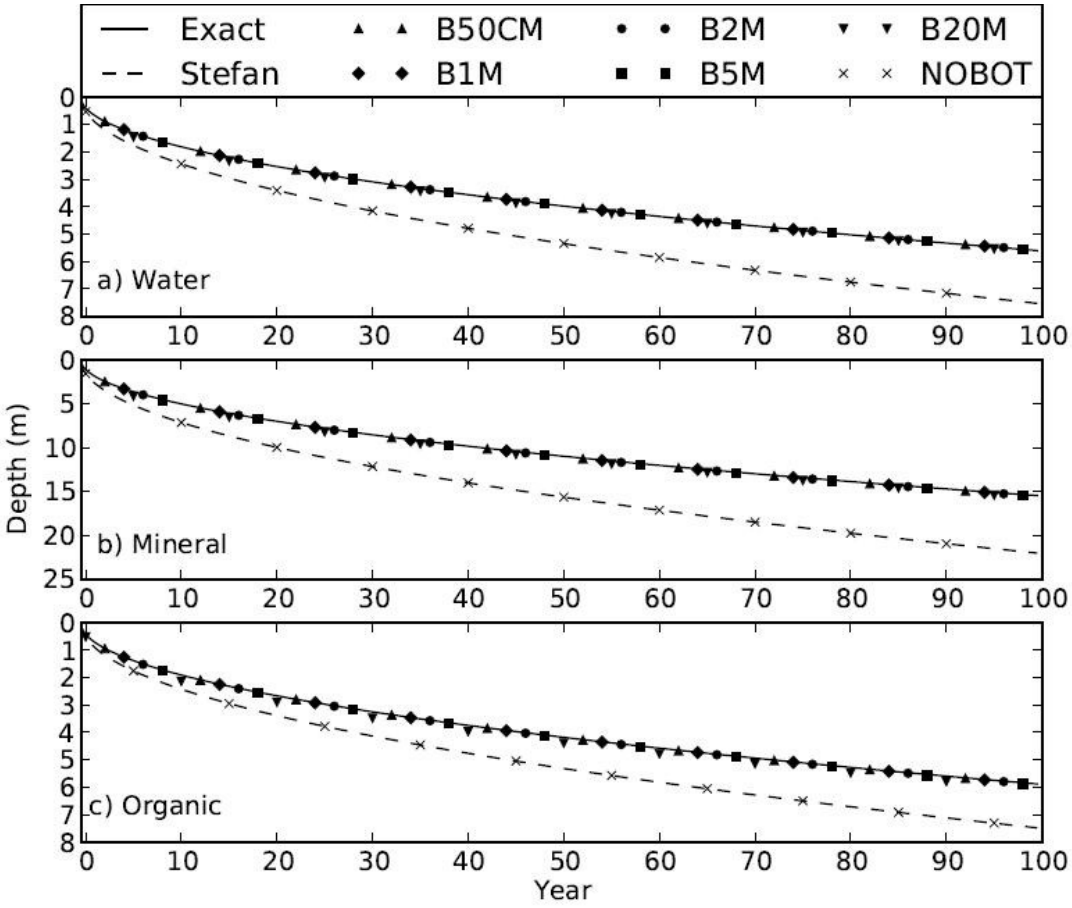

Figure 4. Comparisons of outputs from DOS-TEM simulations (dashed lines) and exact Neumann solutions (solid lines) for a) water, b) mineral soil, and c) organic soil over a period of one hundred years, at depths from 0 cm to 20 m.

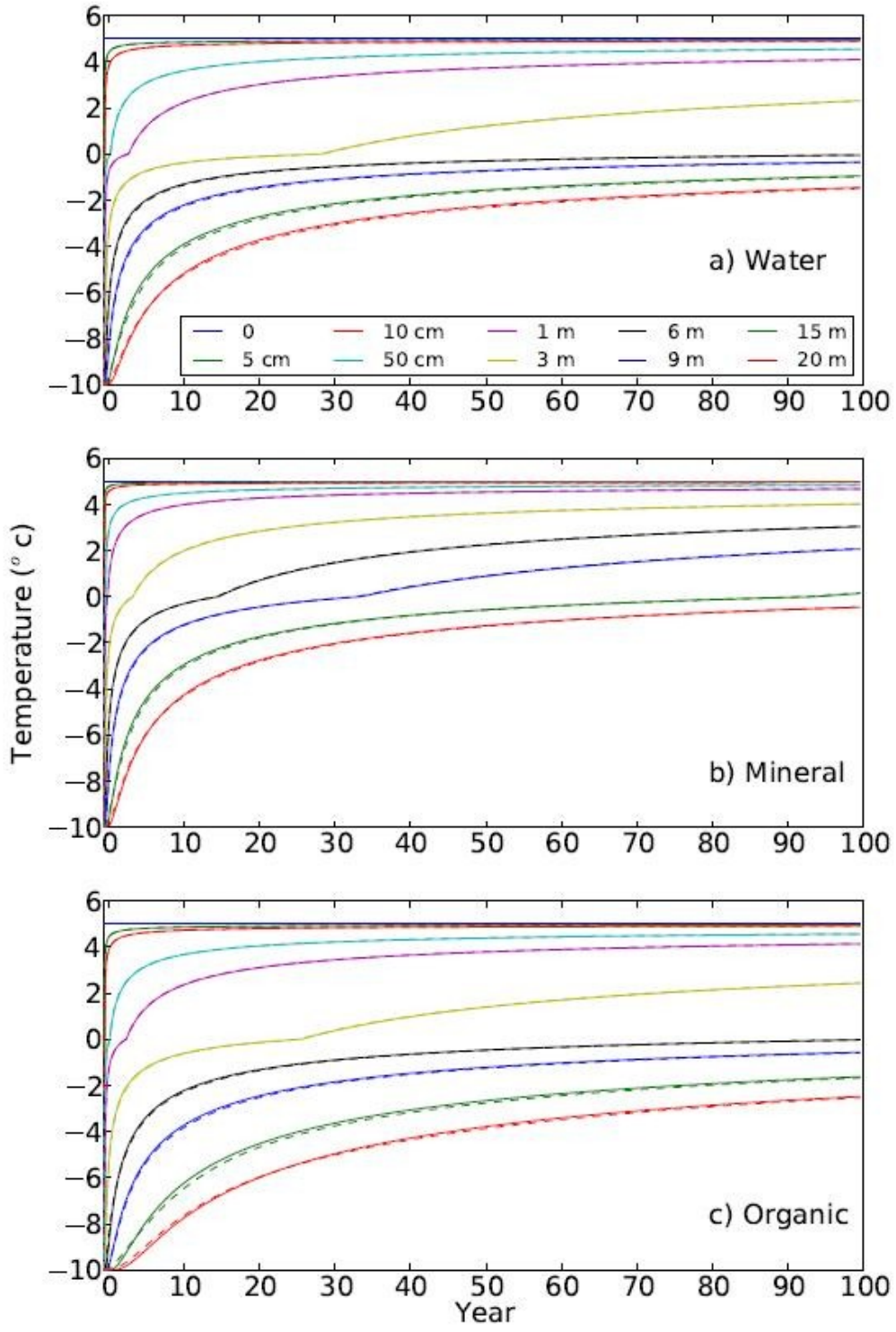

Figure 5. Comparisons of simulated maximum (monthly) snow thicknesses at the *center, rim, pond,* and *lake* sites, the default values (with no maximum snow thickness set), with those from field measurements at the *center* site (center-obs), over the period from 2003 to 2011.

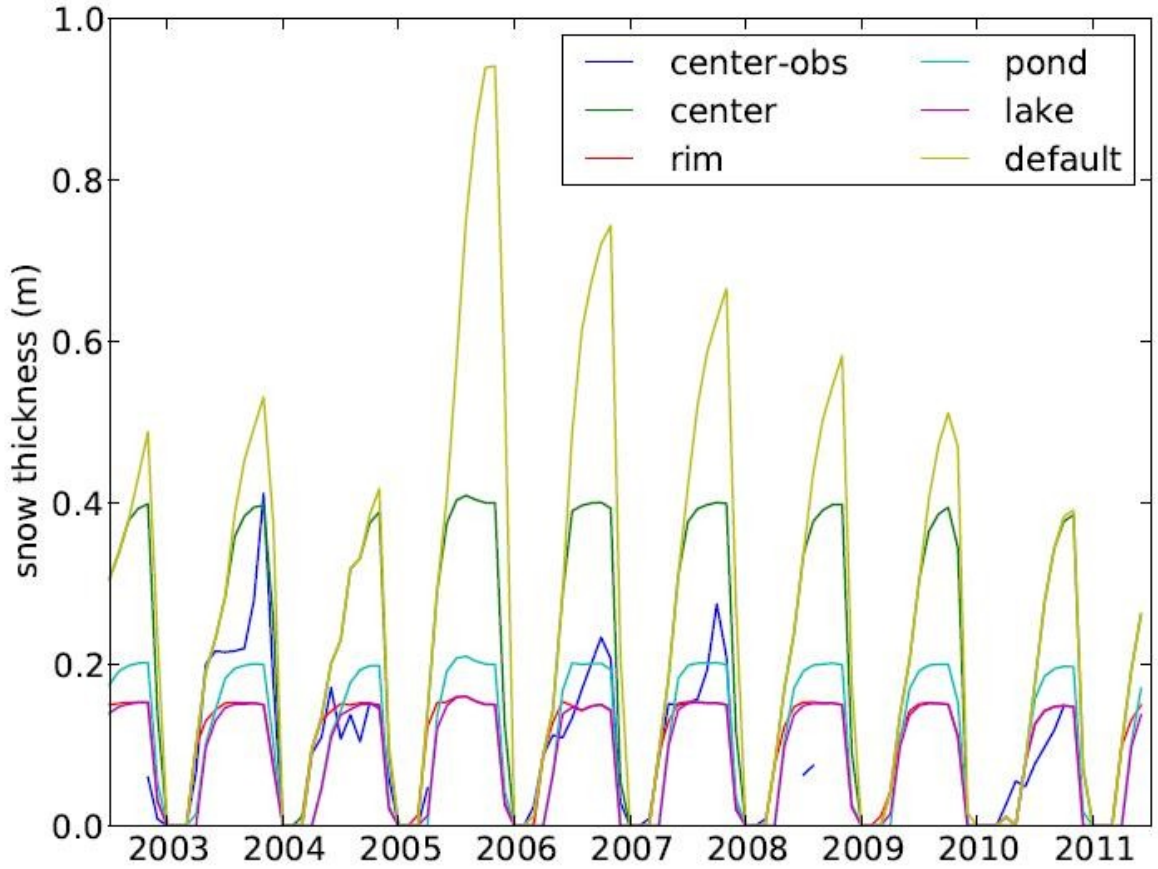

Figure 6. Comparisons of monthly average soil temperatures at 2 cm and 51 cm depth below the *rim* site from simulations (mod), with and without a maximum snow thickness (b and nb), using derived and default thermal properties (der and def), with those from field measurements (obs), over the period from 2003 to 2011.

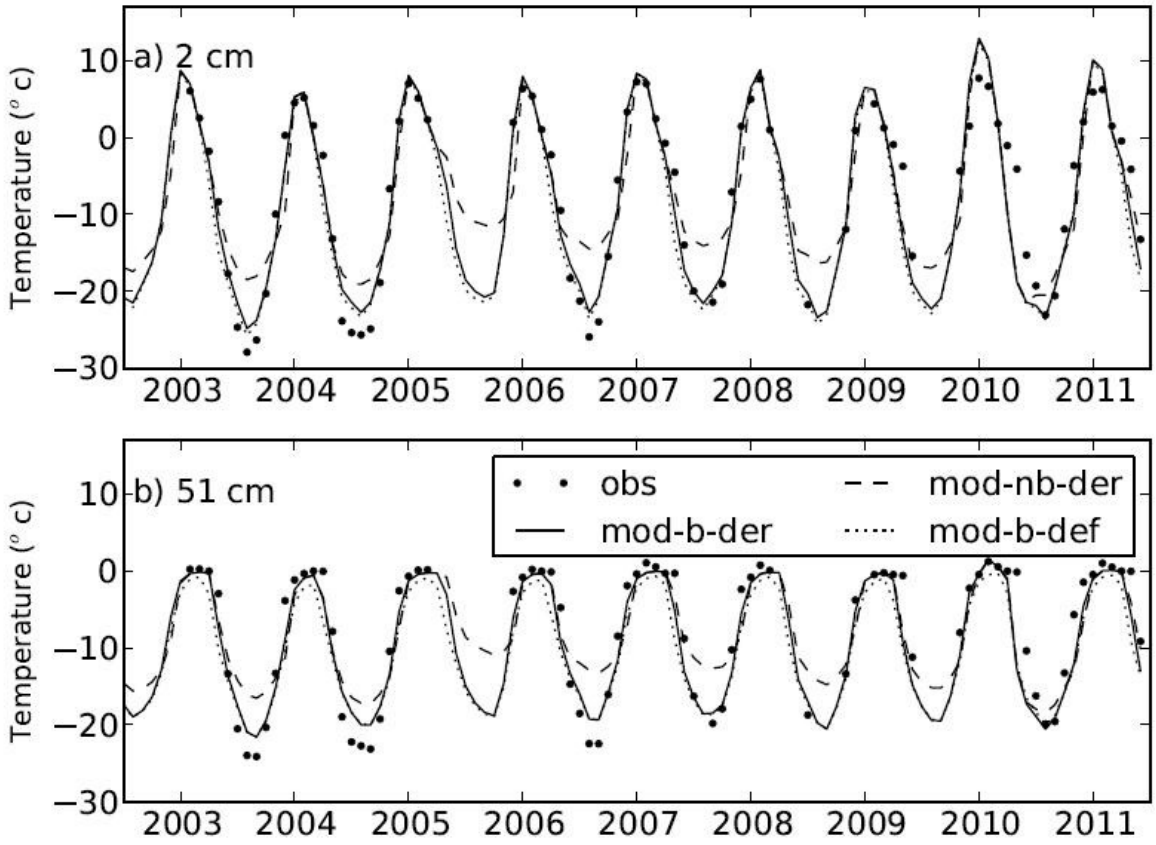

Figure 7. Comparisons of monthly average soil temperatures at 1 and 40 cm depth below the *center* site from simulations (mod) with and without a maximum snow thickness setting (b and nb), using derived and default thermal properties (der and def), with those from field measurements (obs), over the period from 2003 to 2011.

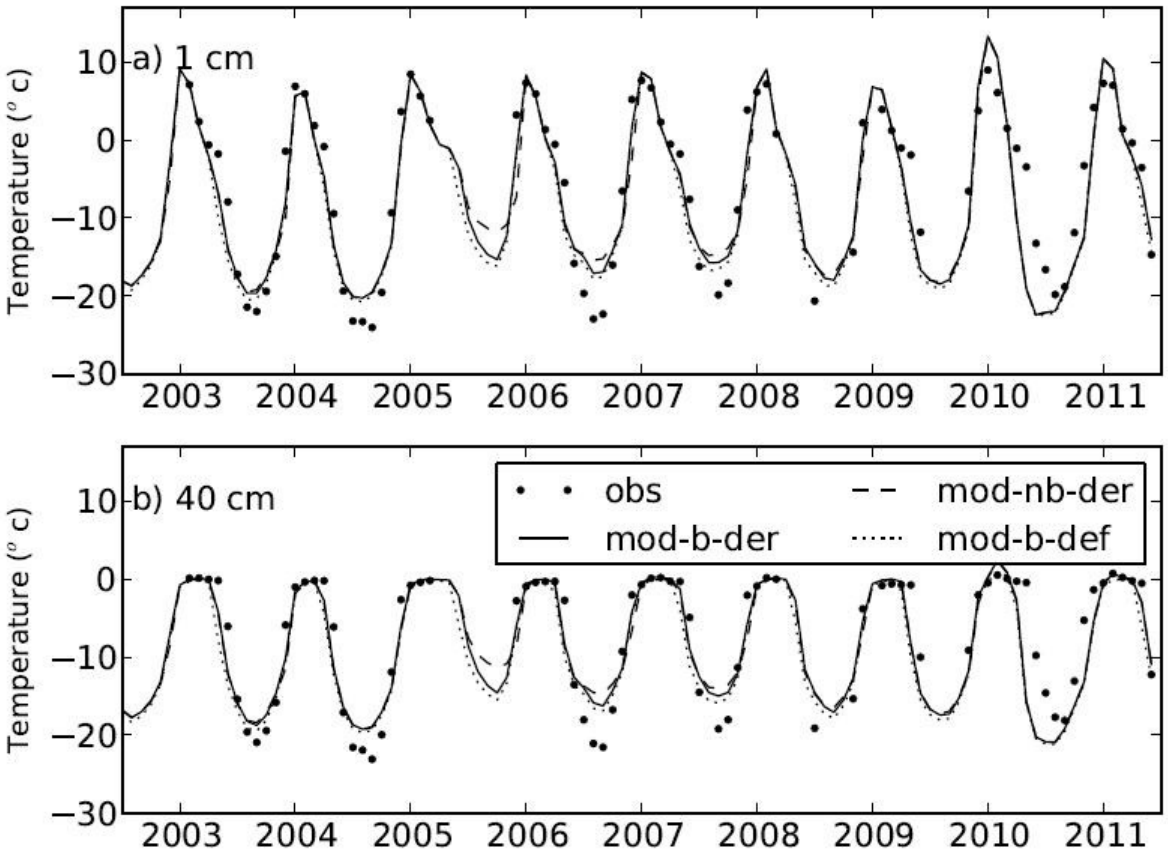

Figure 8. Comparisons of monthly average water temperatures at 1, 69 and 86 cm depth below the water surface at the *pond* site from simulations with 15 cm (mod-15cm) and 2 cm (mod-2cm) maximum snow thickness, over the period from 2007 to 2011.

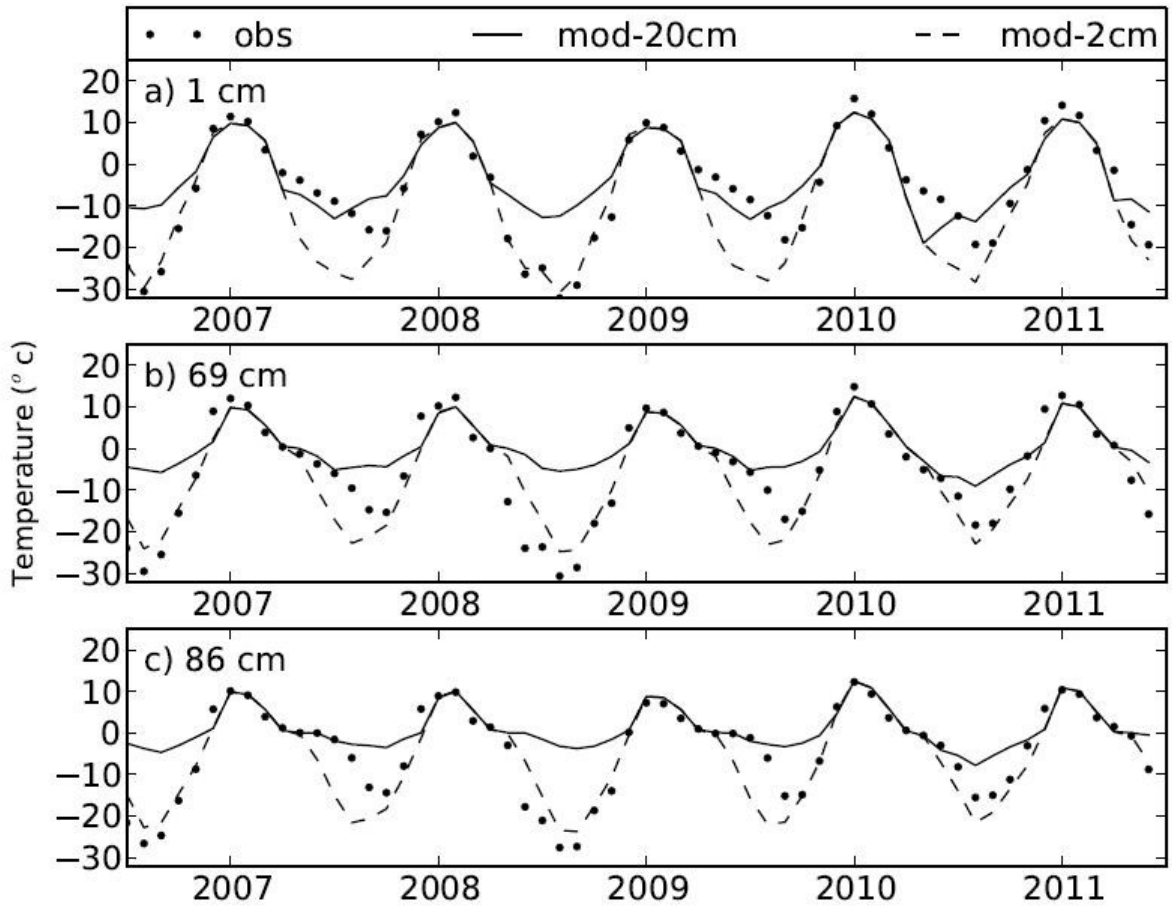

Figure 9. Comparisons of monthly average water temperatures at 2 (a), 4 (b) and 6 m(c) below the water surface at the *lake* site from simulations (mod) using default, 10 times, and 100 times the eddy diffusion coefficient (ke, ke10, and ke100) with field measurements (obs) over the period from 2009 to 2011.

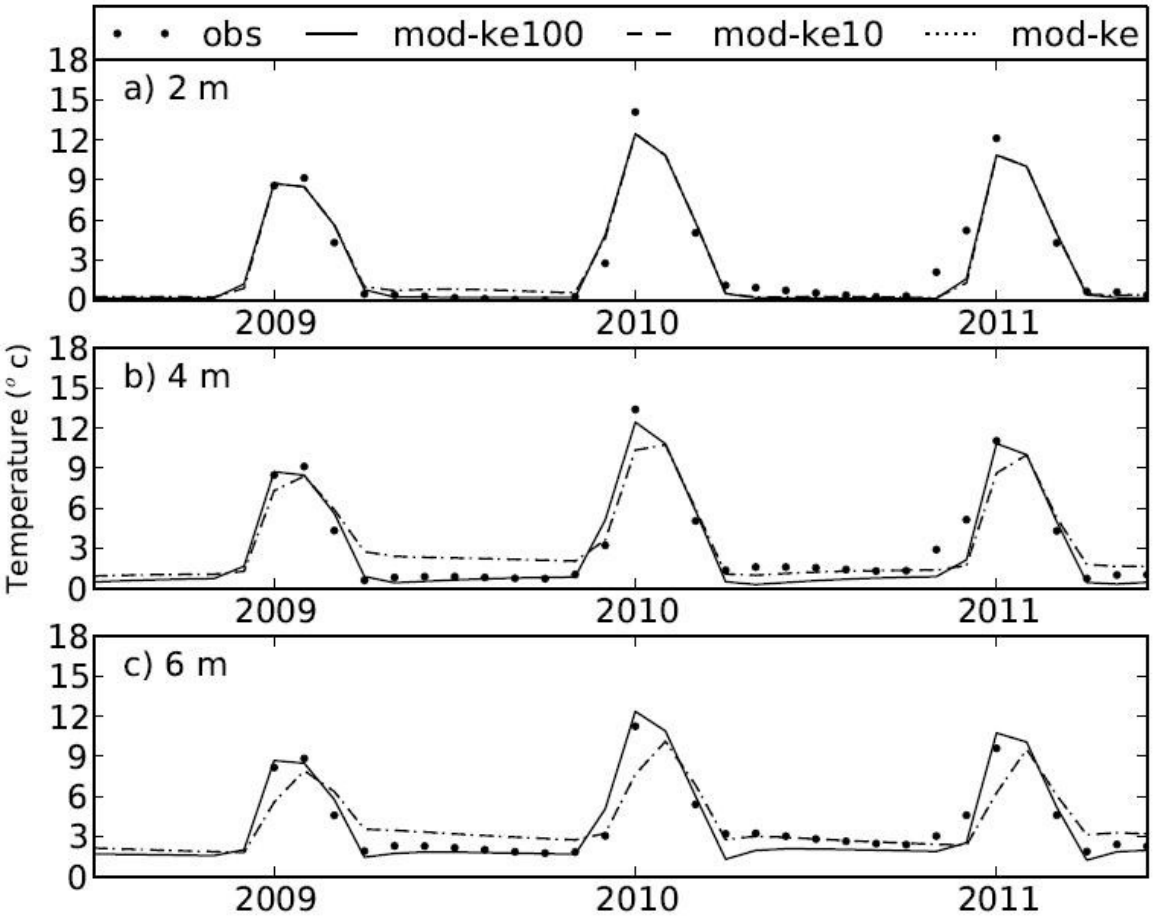

Figure 10. Simulated soil freezing (blue) and thawing (red) fronts, and water freezing (green) and thawing (yellow) fronts (depths in meters) over the period from 2003 to 2011 for a) the *rim* site, b) the *center* site, c) the *pond* site with 15 cm maximum snow thickness, d) the *pond* site with 2 cm maximum snow thickness, and e) the *lake* site. The surface of the soil was taken to be at 0 m depth, with the downward direction positive and the upward direction negative.

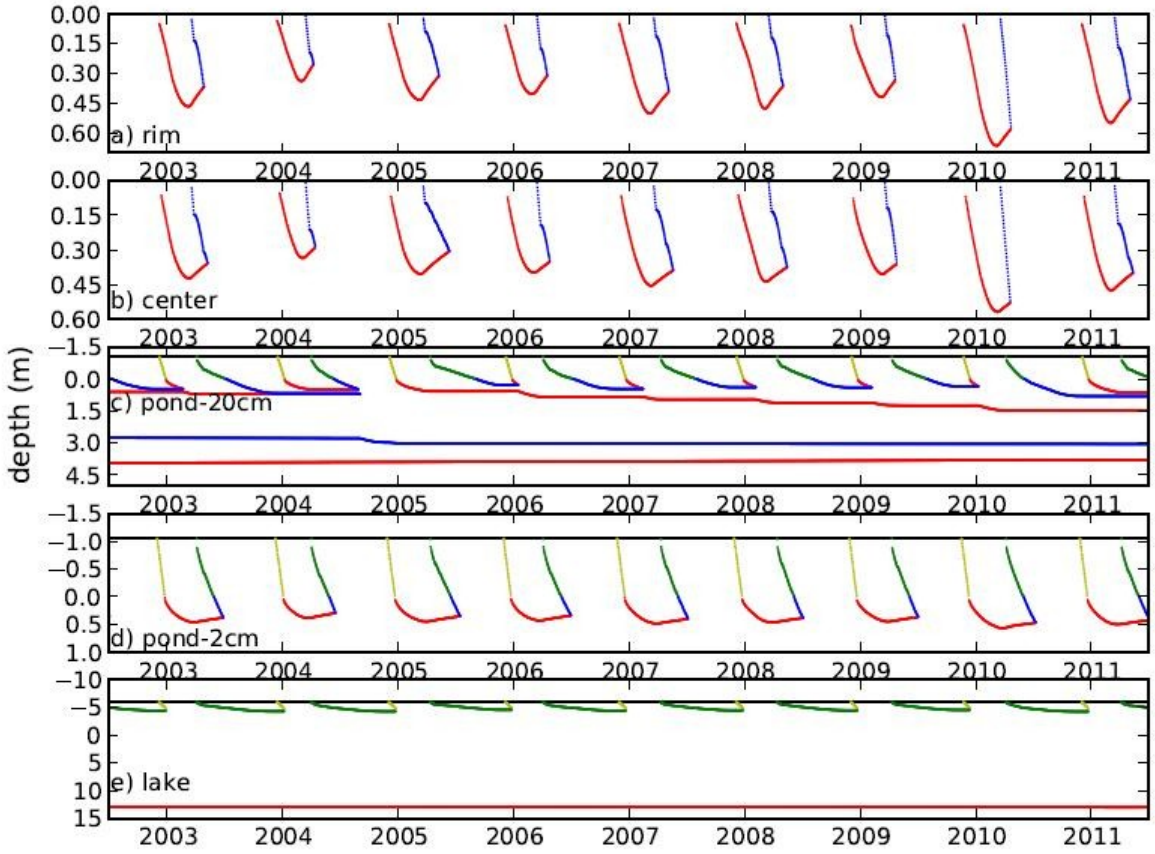

Figure 11. Comparisons between simulated (dashed lines) and measured (solid lines) values for annual mean (green), maximum (red), and minimum (blue) soil temperatures (^{o}C) averaged over the period from 2007 to 2011 for the a) *rim*, b) *center*, c) *pond*, and d) *lake* sites

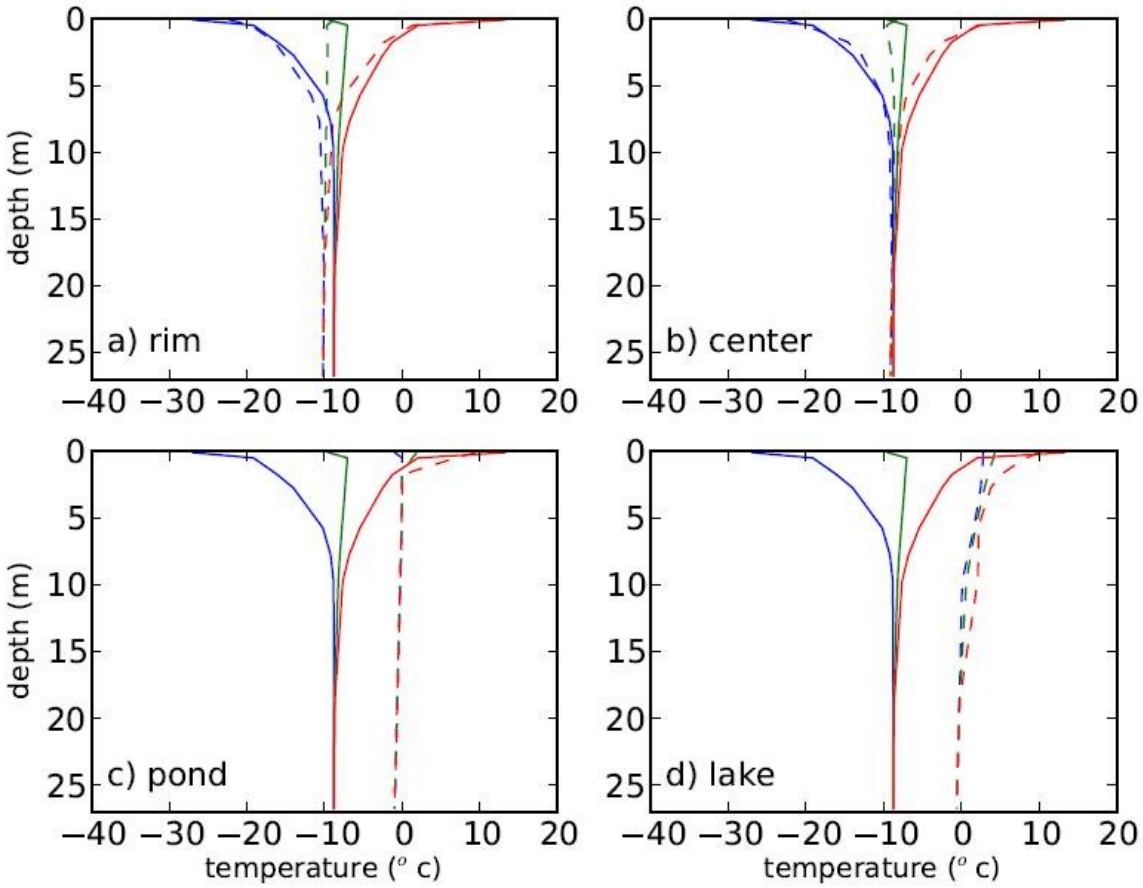

Figure 12. Responses of simulated multi-year mean (2003-2011) unfrozen soil thickness to changes in water depths in a) polygon centers (with maximum water depths of 0.2, 0.6 and 1.2 m) and b) lakes (with maximum water depths of 2.0, 4.0 and 6.0 m).

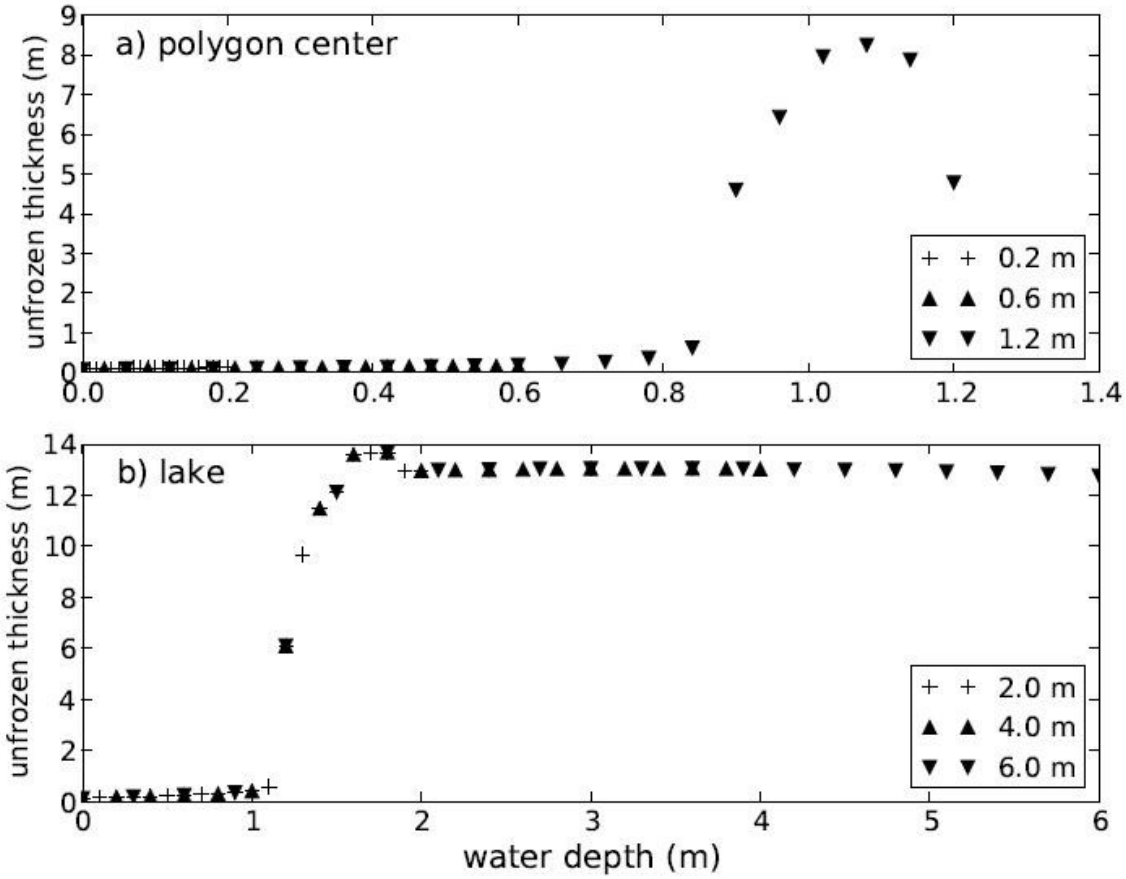

Figure A1. The ground components considered in the DOS-TEM (a), and a diagram of updating freezing and thawing fronts of ground components, together with temperatures (b). DX, TC, HC, and PCE stand for thickness, thermal conductivity, heat capacity, and energy used for phase change, respectively; there are altogether m layers, 1, 2, 3, n and m are layer indexes; DZT and DZB are the distances between the top-down and bottom-up driving depths (dashed and dotted horizontal lines) and the position of the front. Freezing and thawing fronts are indicated with blue and red solid lines, respectively. Vertical dashed lines indicate layers not shown. T_{tb}, T_{bb}, and T_{drv} are the top boundary, bottom boundary and ground surface driving temperatures, respectively. The T_{bb} at the bottom of the ground structure is determined by the temperature and thermal properties of the overlying layer and the prescribed heat flux.

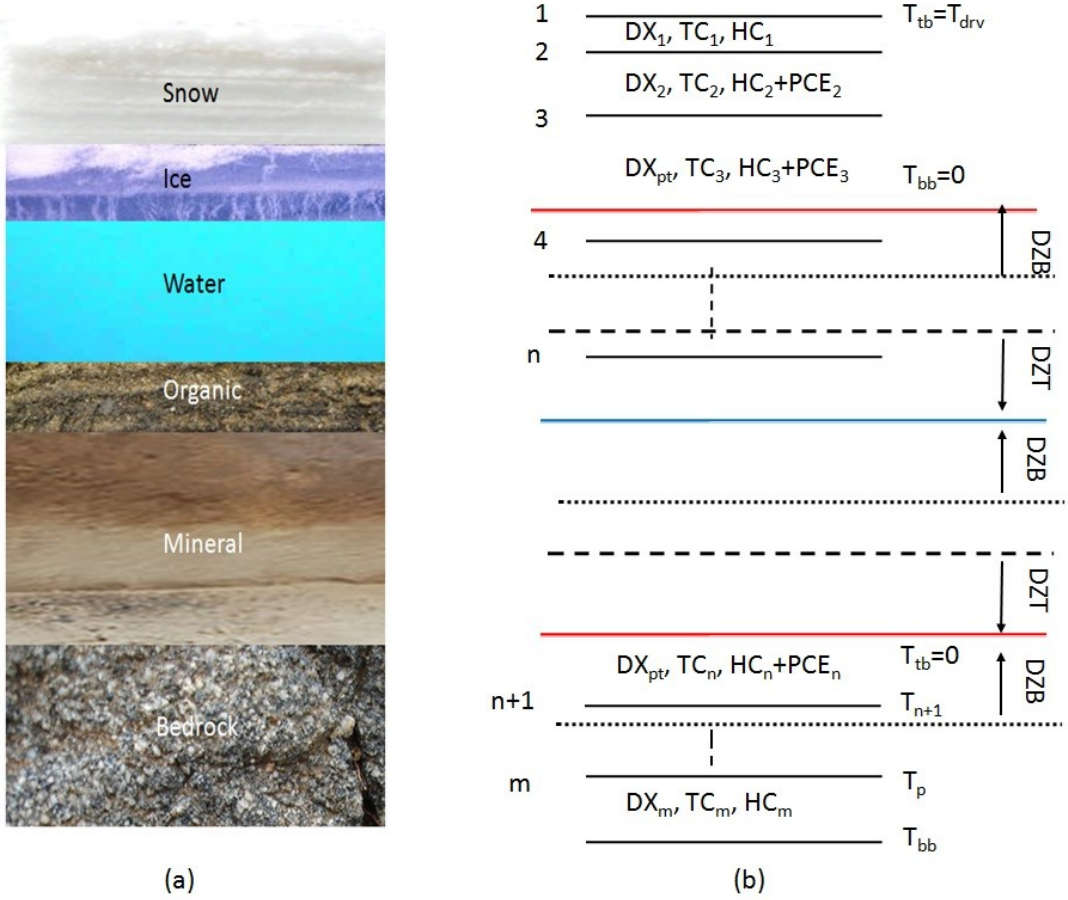

Figure A2. The flowchart for the calculation of upper temperatures for updating the position of the front from above. (note: *Front(s) between position and the front* in the flow chat means there are front(s) between the front under consideration and the position of forcing (DZT above the front).

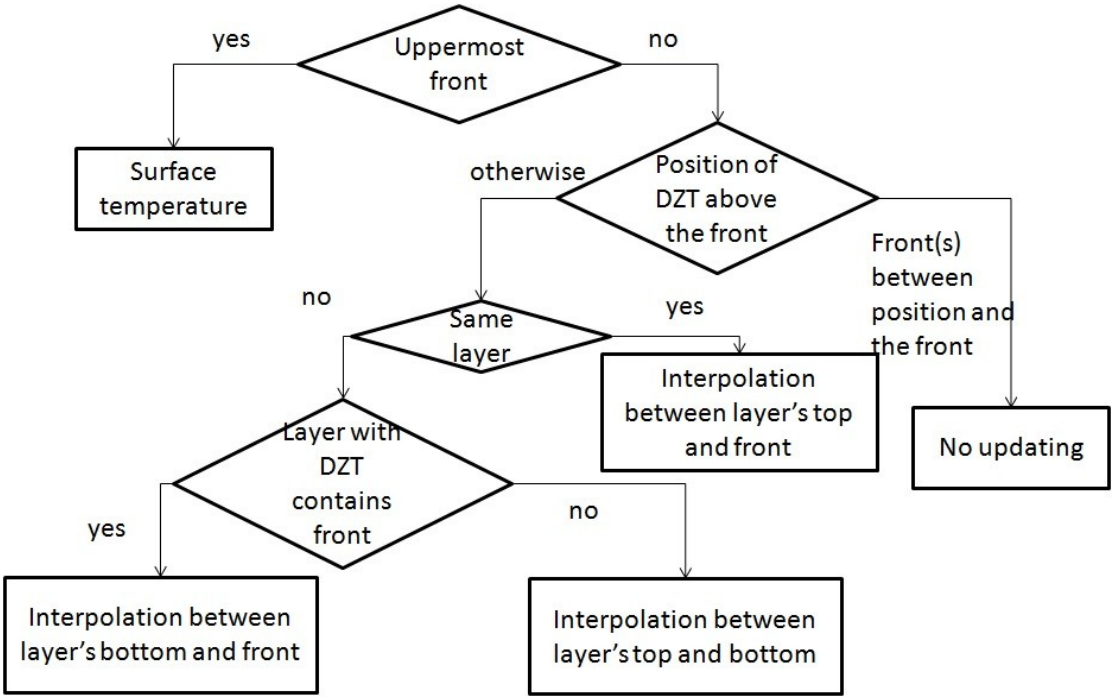

Figure A3. Diagram of rim and pond/lake, in which r_{top} is the radius of the top and rbot that of the bottom of a polygon center or lake; WD , WD_{max} andΔ H are the water depth, maximum water depth, and microtopographic relief height in a polygon center or lake, respectively.